View metadata, citation and similar papers at core.ac.uk

brought to you by CORE

provided by Texas A&M Repository

EVALUATION OF BIOMIMETIC AND ALLOY-BASED MATERIALS FOR ORTHOPEDIC APPLICATIONS

A Dissertation

by

VIVIANA RAQUEL GUIZA-ARGUELLO

Submitted to the Office of Graduate Studies of
Texas A&M University
in partial fulfillment of the requirements for the degree of

DOCTOR OF PHILOSOPHY

Chair of Committee,	Mariah Hahn
Committee Members,	Melissa Grunlan
	Katy Kao
	Victor Ugaz
Head of Department,	M. Nazmul Karim

August 2013

Major Subject: Chemical Engineering

Copyright 2013 Viviana Raquel Guiza-Arguello

ABSTRACT

The basic principle of tissue engineering is the combination of appropriate cells with biomaterials under conditions that promote and lead to tissue formation. A tissue engineering scaffold is a material that supports cells for their growth, proliferation, and differentiation in the absence of native extracellular matrix (ECM). The ECM was originally thought to provide primarily a mechanical support for the cells, but through receptors on the surface of cells, the ECM takes part in promoting cell adhesion, migration, growth, differentiation, and apoptosis. Ideally, a tissue engineered scaffold should mimic both the form and function of native ECM. Additionally, like any other biomaterial for implantation, a tissue engineered scaffold should be biocompatible and not initiate tissue reactions or immune responses.

This work focuses on the evaluation of the biocompatibility of novel alloy-based materials for orthopedic applications. In addition, in the context of bone regeneration, it examines the influence of select native ECM constituents on mesenchymal stem cell (MSC) osteogenic differentiation in 3-D contexts. On the other hand, given the crucial role of vasculogenesis in cell nutrition in the scaffolds, ECM mimics found to support osteogenesis were further evaluated for endothelial cell adhesion and migration. For the hydrogel systems presented in this manuscript, poly(ethylene glycol) diacrylate (PEGDA) networks were selected as the base scaffold due to the broad tunability of their mechanical properties and their previous use in bone regeneration applications. In addition, pure PEGDA hydrogels do not intrinsically promote cell adhesion. Thus, cell

interactions with PEGDA gels are initially isolated to the interactions supported by the proteins tethered to the scaffold.

This work attempts to contribute to the development of novel materials that provide biocompatibility and enhanced versatility in orthopedic applications. Moreover, in the context of bone regeneration, the use of selective ECM biomolecules in hybrid hydrogel scaffolds will aid in the understanding of MSC osteogenic responses to specific ECM constituents. Additionally, incorporation of ECM mimics that support both osteogenesis and vasculogenesis will provide a more controlled platform which will serve as a foundation for the fabrication of more efficient vascularized bone constructs.

DEDICATION

To my brother Juan Pablo, whose company is our endless source of family happiness and love, and whose presence in our lives blesses us all everyday.

To my loving parents Raquel and German as well as my beautiful Daniela, Jairo and Andres, who are the pillars of my strength and motivation to move forward in life.

To Juli, Linix, Silvis and Clementito for their unconditional true friendship and support.

To Camila, Cynthia and Jairo, who will always be my second home.

ACKNOWLEDGEMENTS

I would like to take this opportunity to express my gratitude to the people who have been instrumental in the completion of this work. I would like to express my gratitude to my advisor, Dr. Mariah Hahn, and my committee members, Dr. Melissa Grunlan, Dr.Katy Kao and Dr. Victor Ugaz for their guidance and support throughout my learning process.

I also want to extend my gratitude to Dr. Zhilei Chen, who was willing to participate in my final defense committee at the last moment. Finally, thanks also go to my friends and colleagues for their collaboration and support during the performance of the experimental work.

TABLE OF CONTENTS

CHAPTER Page

LIST OF FIGURES

FIGURE Page

LIST OF TABLES

TABLE Page

CHAPTER I

INTRODUCTION

The basic principle of tissue engineering is the combination of appropriate cells with biomaterials under conditions that promote and lead to tissue formation. A tissue engineering scaffold is a material that supports cells for their growth, proliferation, and differentiation in the absence of native extracellular matrix (ECM). The ECM was originally thought to act primarily as a mechanical support for the cells, but through receptors on the surface of cells, the ECM takes part in promoting cell adhesion, migration, growth, differentiation, and apoptosis [1]. Ideally, a tissue engineered scaffold should mimic both the form and function of native ECM. Additionally, like any other biomaterial for implantation, a tissue engineered scaffold should be biocompatible and not initiate tissue reactions or immune responses.

This work focuses on the evaluation of the biocompatibility of novel alloy-based materials for orthopedic applications. In addition, in the context of bone regeneration, it examines the influence of select native ECM constituents on mesenchymal stem cell (MSC) osteogenic differentiation in 3-D contexts. On the other hand, given the crucial role of vasculogenesis in cell nutrition in the scaffolds, ECM mimics found to support osteogenesis were further evaluated for their capacity to support endothelial cell adhesion and migration. For the hydrogel systems presented in this manuscript, poly(ethylene glycol) diacrylate (PEGDA) networks were selected as the base scaffold due to the broad tunability of their mechanical properties and their previous use in bone

regeneration applications [2-5]. In addition, pure PEGDA hydrogels function as biological ‘‘blank slates’’ in that they do not significantly adsorb cell adhesive serum proteins and therefore do not intrinsically promote cell adhesion [6]. Thus, cell interactions with PEGDA gels are initially isolated to the proteins specifically tethered to the scaffold as well as the interactions supported by these proteins. The specific aims and rationale for this work were the following:

- ***Evaluate the biocompatibility and corrosion resistance of a NiMnSn magnetic shape memory alloy (MSMA) in physiological conditions***. Recently, magnetic shape memory alloys (MSMAs) have emerged as an interesting extension to conventional shape memory alloys (SMAs) due to the capacity of MSMAs to undergo reversible deformation in response to an externally applied magnetic field. As such, MSMAs show substantial promise in biomedical applications for which extracorporeal device activation would be desirable or required. Here we study NiMnSn MSMAs because they allow for high actuation stress and greater toughness compared to conventional MSMAs while still allowing for extracorporeal actuation. However, the cytocompatibility of NiMnSn alloys must be evaluated prior to their use in biomedical applications. In the current work, NiMnSn MSMA cytotoxicity and its relationship to ion release was evaluated using NIH/3T3 mouse fibroblasts encapsulated in 3D poly(ethylene glycol) diacrylate (PEGDA) hydrogels in order to mimic the cellular environment provided by many implant-contacting tissues. Due to the potential cytotoxicity of Ni and

Mn, the effect of a poly(allylamine hydrochloride)/poly(acrylic acid) (PAH/PAA) passivation layer on alloy corrosion and cytocompatibility was also evaluated.

- ***Elucidate the influence of select ECM constituents on mesenchymal stem cell (MSC) osteogenic differentiation in 3-D contexts.*** We incorporated specific ECM molecules into hydrogel scaffolds designed to have moduli within the ‘‘osteogenic’’ range identified in the 3-D human and mouse MSC studies of Huebsch et al. [80]. In selecting molecules for examination, we chose to focus on several ECM proteins associated with bone morphogenesis and /or bone fracture healing toward the goal of identifying scaffolds with intrinsically osteoinductive properties. These proteins were then conjugated into poly(ethylene glycol) diacrylate (PEGDA) hydrogel networks. 10T½ MSCs were encapsulated within PEGDA hydrogels containing defined amounts of fibronectin (FN), fibrinogen (FG) or laminin-1 (LN). The levels of various markers of osteoblast, chondrocytic, smooth muscle cell and adipocytic fates were then monitored with time in culture toward assessing the strength and specificity of observed osteogenic responses.
- ***Evaluate endothelial cell adhesion and migration on biomimetic hydrogels for the fabrication of tissue-engineered vascularized bone constructs***. The results from the previous studies suggested that α1 and α2 integrin cell adhesion is probably involved in mesenchymal stem cell osteogenesis. Nonetheless, in this particular case, the complexity of the interplay among the multiple signals provided to the cells made it difficult to determine whether α1 and α2 integrin adhesion was responsible for the differentiation profiles observed. The ideal

system for evaluating the effect of a specific signal on cell behavior would allow the incorporation of the desired signaling in an appropriate three-dimensional (3D) protein structure without the additional signals associated with the biopolymer. Recent studies conducted in our lab employed a novel biomaterial platform based on a collagen-mimetic protein derived from group A Streptococcus, Scl2.28, which maintains the native triple helical structure of native collagen and allows the incorporation of desired integrin-binding motifs. Following the development of two Scl2 "daughters" (Scl2-2 or DC2, and Scl2-3 or DC3), which incorporate α1β1 and/or α2β1 integrin-binding motifs based on the collagen sequences GF/LOGER [7, 8], our lab has been able to show that hybrid PEGDA-Scl2 hydrogels support human MSC (hMSC) osteogenic differentiation, and therefore, have the potential to be used as osteoinductive scaffolds. Nonetheless, bone replacement materials are more effective if they also support capillary formation in addition to osteogenesis [9, 10]. Thus, a bone regeneration scaffold must be able to support endothelial cell (EC) adhesion and migration. Therefore, given that DC2 and DC3 incorporate α1β1 and/or α2β1 integrin-binding motifs, and that such motifs are involved in EC adhesion and phenotype in native vessels, the aim of this study was to evaluate the ability of our PEGDA-DC hybrid systems to promote EC adhesion, spreading and migration towards the fabrication of improved vascularized bone constructs.

The achievement of these goals attempts to contribute to the development of novel materials that provide not only biocompatibility, but also innovative features, such as

metamagnetism, which will increase material versatility in orthopedic applications. Moreover, in the context of bone regeneration, the use of select ECM biomolecules in hybrid hydrogel scaffolds will aid in the understanding of MSC osteogenic responses to specific ECM constituents. Additionally, incorporation of ECM mimics such as the Scl2 proteins, which support both osteogenesis and vasculogenesis, will provide a more controlled platform which will serve as a foundation for the fabrication of more efficient vascularized bone constructs for orthopedic applications.

CHAPTER II

EVALUATION OF POLYELECTROLYTE COATINGS ON NIMNSN METAMAGNETIC SHAPE MEMORY ALLOY CYTOTOXICITY AND ION RELEASE

2.1. OVERVIEW

Recently, magnetic shape memory alloys (MSMAs) have emerged as an interesting extension to conventional shape memory alloys (SMAs) due to the capacity of MSMAs to undergo reversible deformation in response to an externally applied magnetic field. As such, MSMAs show substantial promise in biomedical applications for which extracorporeal device activation would be desirable or required. Here we study NiMnSn MSMAs because they allow for high actuation stress and greater toughness compared to conventional MSMAs while still allowing for extracorporeal actuation. However, the cytocompatibility of NiMnSn alloys must be evaluated prior to their use in biomedical applications. In the current work, NiMnSn MSMA cytotoxicity and its relationship to ion release was evaluated using NIH/3T3 mouse fibroblasts. To assess cytocompatibility, NIH/3T3 cells were encapsulated in 3D poly(ethylene glycol) diacrylate (PEGDA) hydrogels in order to mimic the cellular environment provided by many implant-contacting tissues. Due to the potential cytotoxicity of Ni and Mn, the effect of a polyelectrolyte passive coating on alloy corrosion and cytocompatibility was also evaluated. Results indicate that the use of a poly(allylamine hydrochloride)/poly(acrylic acid) (PAH/PAA) passivation layer applied using layer-by-

layer (LbL) assembly significantly increased the cytocompatibility of NiMnSn SMAs via reducing ion release. To our knowledge, this study presents the first cytotoxicity evaluation of NiMnSn MSMAs and lays the groundwork for further biological evaluation of these materials.

2.2. INTRODUCTION

Recently, magnetic shape memory alloys (MSMAs) have emerged as an interesting extension to conventional shape memory alloys (SMAs) due to the capacity of MSMAs to couple magnetic and electrical energy to mechanical work. Conventional SMAs can undergo relatively large recoverable strains as a result of a reversible martensitic phase transformation. These recoverable stains can be triggered by changes in temperature, leading to actuators, or by stress, leading to pseudoelasticity [11-16]. The pseudoelastic response provides a powerful biomedical device design tool unavailable in stainless steels and other traditional metallic materials [12] while the actuator response allows potential for use in micropumps and displacement-stimulated tissue remodeling. However, the need for lead wires and temperature changes for actuation limits the potential biomedical applications of these alloys.

In contrast, MSMAs can undergo reversible deformation in response to an externally applied magnetic field [17-22]. As such, MSMAs may hold significant promise for biomedical applications where extracorporeal device activation is desirable or required. Nickel-Manganese-Gallium (NiMnGa) alloys have been one of the most extensively studied MSMA systems [23-30] due in part to their high recoverable strains

(up to 10%). Nonetheless, NiMnGa MSMAs tend to be brittle, and the sub-physiological temperature range at which NiMnGa alloys displays magnetic shape memory properties limits its potential utility in biomedical applications.

Recently, the alloy ternary series NiMnX (X = Al, In, Sn and Sb) has emerged as a class of MSMAs that exhibit higher transition temperatures than NiMnGa alloys, some close to physiological temperatures [31, 32]. Additionally, NiMnX alloys have the capacity to impose stresses up to 10 times greater than those exhibited by NiMnGa alloys and sintered NiMnSn-based alloys show increased toughness [33, 34]. This is due to the increased amount of magnetic energy available for actuation in NiMnX MSMAs relative to MSMA such as NiMnGa, a trait referred to as meta-magnetism [31]. However, the cytocompatibility of NiMnX alloys must be tested in order to further evaluate their potential for biomedical applications. This is particularly the case as previous in vitro testing has shown NiMnGa to be cytotoxic [35, 36], and a range of studies have demonstrated the toxicity of both Ni [37-41] and Mn [42, 43]. In the present study, we therefore examined the cytotoxicity of the NiMnSn member of the broader NiMnX (X = Al, In, Sn and Sb) MSMA family. Sn was selected over In and Sb as the tertiary alloy component due to the high cytotoxicity of In and Sb relative to Mn, Ni, and Sn [44] as well as the increased toughness of sintered NiMnSn alloys relative to NiMnGa MSMAs [45]. Furthermore, Sn was selected over Al due to the smaller thermal hysteresis of the martensitic transformation [46].

To assess the cytocompatibility of NiMnSn alloys, NIH/3T3 cells mouse fibroblasts, a cell line commonly used in cytotoxicity studies [47-50], were encapsulated

in three-dimensional (3D) poly(ethylene glycol) diacrylate (PEGDA) hydrogels in order to mimic the cellular environment provided by many implant-contacting tissues. Furthermore, potential improvements in alloy cytocompatibility following layer-by-layer (LbL) application of a poly(allylamine hydrochloride)/poly(acrylic acid) (PAH/PAA) were evaluated. Specifically, PAH/PAA coatings have previously been shown to significantly improve the corrosion resistance of aluminum [51] and to reduce the transport of multivalent ions [52]. Additionally, thin PAH/PAA coatings have also been shown to withstand the large cyclic deformations associated with martensitic transformation on NiTi substrates [53, 54]. For both coated and uncoated NiMnSn MSMAs, cytotoxicity assessments were correlated with alloy ion release measures to understand the primary source of observed cytotoxicity. To our knowledge, this study presents the first cytotoxicity evaluation of NiMn-based MSMAs with and without a polyelectrolyte passive coating.

2.3. MATERIALS AND METHODS

2.3.1. Alloy fabrication

Specimens 10x10x1 mm^3 were cut from NiMnSn pre-alloyed bulk ingots (50 at% Ni, 39 at% Mn, and 11 at% Sn) via wire electro-discharge machining (EDM). Similarly, 10x10x1 mm^3 specimens were cut from Ni (99.999% pure) and Ti (commercially pure grade 2) bulk ingots using EDM. A diamond saw was used to cut 10x10x1 mm^3 specimens from Mn (99.9% pure) chips and Sn (99.8% pure) foil. NiMnSn alloys were homogenized at 900C for 24 hours under argon in a sealed quartz ampule. All 10x10x1

mm^3 alloy specimens were then polished to a 0.3 μm finish using silicon carbide paper followed by alumina colloidal powder on all sides.

2.3.2. Polyelectrolyte coating fabrication

Two sets of homogenized NiMnSn samples were coated using layer-by-layer assembly via dip-coating. Commercially pure grade 2 Ti wire was glued to one sample edge using Loctite M-21HP medical device epoxy (ISO 10993 compliant) to allow even dip-coating. Aqueous solutions were prepared using 18.2 MΩ deionized water. Individual solutions containing either 0.1 M of PAA (Sigma Aldrich, Mw ~ 100, 000 g/mol) or 0.1 M PAH (Sigma Aldrich, Mw ~ 15, 000 g/mol) were rolled overnight to allow for full dissolution. Both solutions were altered to a pH of 4.5 using 0.1 M NaOH solution prior to deposition. Samples were coated with 10 bilayers (BLs) of PAH/PAA via LbL processing. One set of coated NiMnSn samples was exposed to 180C for 5 h under Ar to induce crosslinking of the PAH/PAA coating, while the second set was not exposed to thermal crosslinking.

To measure coating thickness, P-doped, single-side polished, <1 0 0> silicon wafers (University Wafer), each with a thickness of 500 μm, were used as substrates for ellipsometric thickness measurements. Film thicknesses were measured using a Model alpha-SE Ellipsometer (J.A. Woollman Co., Inc) with a 632.8 nm laser and a 70º incidence angle. Thermal crosslinking yielded a reduction in coating thickness - 10 BL coatings measured 38.0 nm thick prior to heat treatment and 27.8 nm post treatment.

2.3.3. Cell culture studies

Cryopreserved NIH/3T3 cells (ATCC) at passage 4 were thawed and expanded at 37C and 5% CO_2. During expansion, cells were cultured in Dulbecco's Modified Eagle's Medium (DMEM; Hyclone) containing 5% iron-supplemented bovine calf serum (BCS; Hyclone). Cells at passage 8-9 were harvested for the alloy toxicity studies. To evaluate the cytocompatibility of the various metal specimens, harvested NIH/3T3 cells were encapsulated in 3D PEGDA hydrogels in order to mimic the cellular environment provided by many implant-contacting tissues. PEGDA gels were selected for the present studies due to their established cytocompatibility and widespread use as 3D culture platform [55-57]. The resulting cell-laden hydrogels were then cultured in the presence of alloy specimens or metal controls (Ni, Mn, Sn) for a period of 14 days, as described in the following sections.

2.3.3.1. Polymer synthesis

PEGDA was prepared by combining 0.1 mmol/mL dry PEG (6 kDa; Sigma), 0.4 mmol/mL acryloyl chloride, and 0.2 mmol/mL triethylamine in anhydrous dichloromethane (Fisher Scientific) under argon overnight and purified as previously described [58]. Cell adhesion peptide NH_2-Arg-Gly-Asp-Ser-COOH (RGDS; American Peptide) was reacted with acryloyl-PEG-N-hydroxysuccinimide (ACRL-PEG-NHS, 3.4 kDa; Nektar) at a 1:1 molar ratio for 2 h in 50 mM sodium bicarbonate buffer, pH 8.5. The product (ACRL-PEG-RGDS) was purified by dialysis, lyophilized, and stored at -80C until use.

2.3.3.2. Hydrogel preparation and culture

A hydrogel precursor solution was prepared by dissolving PEGDA at 10 wt% in phosphate buffered saline (PBS, pH 7.4; Sigma), after which 10 µl/mL of photoinitiator (260 mg/mL of 2-hydroxy-4'-(2-hydroxy-ethoxy)-2-methyl-propiophenone in 70% ethanol) was added. ACRL-PEG-RGDS was then dissolved in the precursor solution so that the concentration of RGDS in the swollen hydrogels would be 1 µmol/g gel. Following sterile filtration of the precursor solution, NIH/3T3 cells were added at $3x10^6$ cells/mL. This cell suspension was poured into a 1 mm thick rectangular mold and polymerized by 6 min exposure to longwave UV light (~6 mW/cm^2, 365 nm). This polymerization process has previously been demonstrated to be cytocompatible and to result in gels with homogenously distributed cells [55-57]. The resulting hydrogel was removed from the mold, rinsed with PBS, and immersed in DMEM supplemented with 5% BCS and 1% PSA (PSA: 10,000 U/mL penicillin, 10,000 mg/L streptomycin, and 25 mg/L amphotericin; Hyclone) at 37C/5% CO_2.

After 24 h to allow for equilibrium swelling, the hydrogel slab was separated into uniform gels discs using an 8 mm biopsy punch (Miltex). Each disc was transferred to a distinct 12-well culture insert fitted with porous membrane (BD Biosciences). The metallic specimens (number of specimens: n = 4 per metallic formulation) were placed in the bottom of separate wells of a 12-well culture plate. All metallic surfaces were sterilized by immersion in 70% ethanol in water for 1 h and rinsed with sterile de-ionized water. It is anticipated that room temperature ethanol immersion will have

minimal effect on metal surface composition due to the avoidance of oxidative agents, irradiation, and heat.

Following transfer of the gel-laden culture inserts to separate wells of the metal-containing 12-well plate, 1.5 mL of DMEM supplemented with 5% BCS and 1% PSA was added to each well. After 24 h of culture at 37C/5% CO_2, the media surrounding each sample was fully exchanged, after which full media changes were performed every two days. In an initial set of studies, PEGDA hydrogels were exposed to uncoated NiMnSn alloys or to Mn, Ni, or Sn controls. At days 1, 5, and 7 of culture, aliquots of culture media were collected from each sample for ion-release analyses prior to scheduled media changes. The hydrogel discs were similarly harvested at day 7 for comparative cell viability assessments. PAH/PAA-coated and uncoated NiMnSn alloys were then compared in a second set of cell culture experiments. In these studies, aliquots of culture media were collected from each sample for ion-release analyses prior to scheduled media changes at days 1, 7, 10 and 14 of culture. The hydrogel discs were similarly harvested at day 14 for cell viability assessments.

2.3.3.3. Ion release

Levels of Ni, Sn, and Mn ions released from the cultured alloy samples were monitored using Inductively Coupled Plasma Emission-Mass Spectroscopy (ICP-MS). At the time of analysis, collected media samples were diluted 1:10 v/v with 1% HNO_3. Ion concentrations were measured using a Perkin Elmer NexION 300 relative to

standards prepared from cell culture media containing known amounts of Ni, Sn, or Mn (Inorganic Ventures, $\geq$ 99.89% purity).

2.3.3.4. Cell viability

Measures of DNA are standardly considered indicators of net cell proliferation and death [58]. This is because DNA from dead cells is rapidly degraded (and therefore not detected by standard DNA assays) and since each normal somatic cell contains a specific amount of DNA. To analyze DNA levels within each metal-exposed hydrogel sample, gel discs ($n = 4$ per metal formulation) collected at the study endpoint were digested for 24 h at 37C in 1 ml of 0.1 M NaOH per 0.2 g hydrogel wet weight. The samples were then centrifuged (10,000 g for 10 min), neutralized, and their DNA content determined using the PicoGreen assay (Invitrogen). Calf thymus DNA (Sigma) encapsulated within PEGDA hydrogels and exposed to the same digestion conditions as the samples served as a standard.

2.3.4. Statistical analyses

Data are reported as mean ± standard error of the mean. Comparison of sample means was performed using analysis of variance (ANOVA) followed by a Tukey's post-hoc test, $p < 0.05$ (SPSS software).

2.4. RESULTS

2.4.1. Cell viability and ion release studies

Cell behavior is often dependent on environmental conditions, and phenomena observed in 3D culture systems are not necessarily reflected in 2D culture studies [59, 60]. Therefore, to more closely mimic the environment of many implant-contacting tissues, the cytotoxicity studies were performed on NIH/3T3 cells encapsulated within 3D PEGDA hydrogels. DNA measures are standardly considered indicators of cell viability as cellular DNA is rapidly degraded (and therefore undetected by standard assays) following cell destruction. Thus, shifts in sample DNA levels with time reflect net cell proliferation and death [56, 58]. **Figure 1** shows the results from initial cell toxicity studies designed to compare NiMnSn alloy toxicity relative to that of its individual components. Viability was significantly lower for cells exposed to NiMnSn relative to cells exposed to Sn (statistical significance level: $p = 0.004$) and relative to cells without metal/alloy exposure ("media only" samples, $p < 0.001$). Similarly, Ni samples were as cytocompatible as the PEG-only controls over the culture period of 10 days. However, cells exposed to pure Mn samples appeared to be of reduced viability relative to media only controls, and levels of cell viability in pure Mn samples could not be statistically distinguished from those of NiMnSn samples.

In order to gain insight into the observed cell toxicity results, ion leaching data was examined via ICP-MS (**Figure 2**). In interpreting the data in **Figure 2**, it is important to recall that culture media surrounding the alloys was exchanged every 2 days following day 1 of culture. This process was intended to mimic the process of fluid

exchange/circulation that occurs in natural body tissues. The Mn ion levels released into the NiMnSn culture media over the 7 day culture period were relatively constant at approximately 700 ppb. In contrast, ICP-MS revealed an initial burst release of Mn ions from the Mn control. However, by day 4, the Mn ion levels released from the NiMnSn alloys were approximately 60% of the levels released from pure Mn sample (**Figure 2A**).

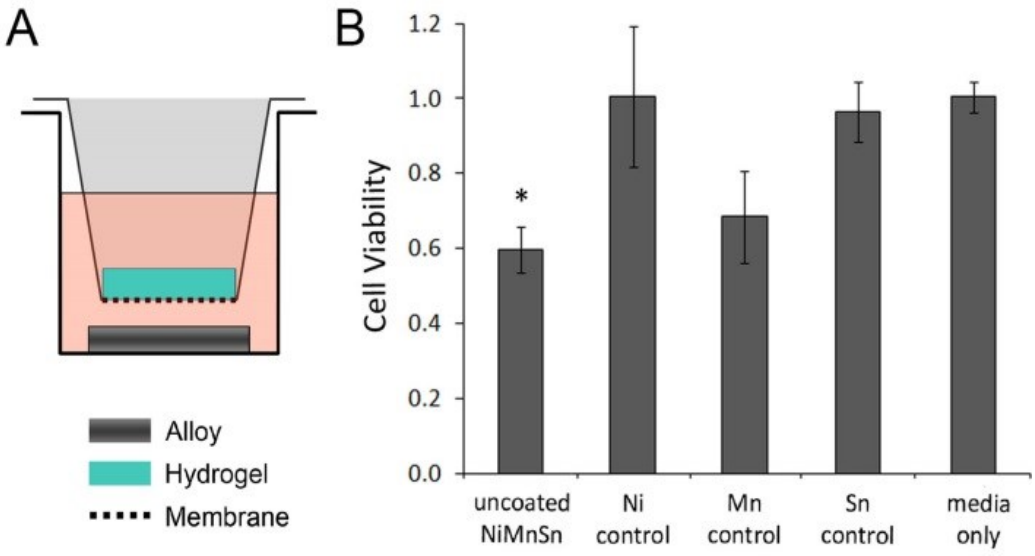

Figure 1. (A) Schematic of the cytoxicity testing setup. (B) Cytotoxicity of uncoated NiMnSn alloys relative to Ni, Mn, Sn, and culture media (no metal sample) controls as evaluated by DNA assessments. For ease of comparison, results are normalized to the media controls. *, significantly different from the corresponding Sn, Ni, and media samples, $p < 0.05$.

The release of Ni ions from the NiMnSn samples appeared to be greater than that from pure Ni. This may be due to the oxide layer associated with pure Ni acting as a greater barrier to Ni release than the oxide layer of NiMnSn. In any case, Ni ion levels in the culture media of both Ni metal were approximately 500-650 ppb, whereas that in the

NiMnSn ranged from 700-900 ppb. Results for Sn ions indicate initial release levels around 500-600 ppb that drop continuously over the experimental timeframe.

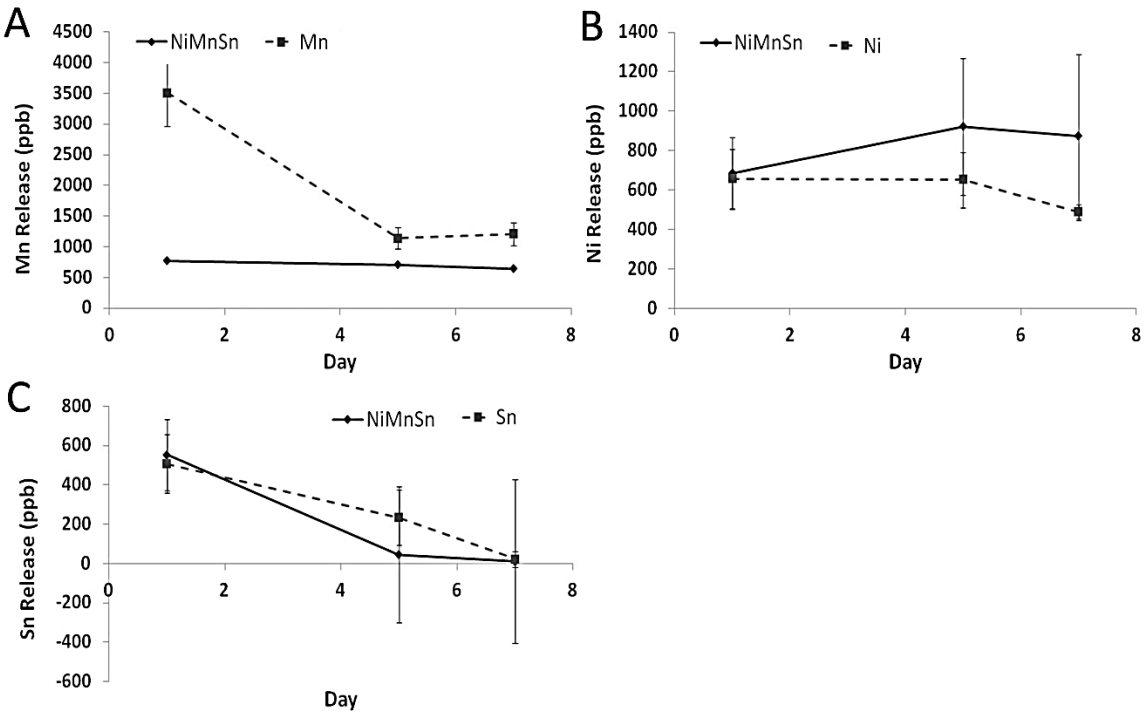

Figure 2. Mn, Ni and Sn ion release from the NiMnSn alloys and the Mn, Ni and Sn controls per ICP-MS measures. Media surrounding each metal specimen was fully exchanged every 2 days beginning at day 1 of culture.

Comparison of the present results with existing literature is challenging due to the dependency of ion toxicity thresholds on cell type and due to the number of ions involved (Ni, Mn, Sn). In comparing our data to literature, we have therefore chosen to focus on a cell line of similar sensitivity as NIH/3T3 mouse fibroblasts, namely MC3T3-E1 mouse cells. MC3T3-E1 mouse cells are one of only two cell types whose viability has been evaluated under consistent methods for 43 different metal ions, each ion at multiple concentrations. Literature indicates that Sn ions cytotoxicity is not observed for

MC3T3-E1 cells until Sn exceeds approximately 2 ppm or 60 ppm, depending on whether the Sn ions are 2^+ or 4^+ respectively [44]. These results are consistent with the high MC3T3-E1 cell viability observed for hydrogels in contact with Sn metal controls, where released Sn ions were 10-to-250 fold below these toxicity limits. Similarly, literature on Ni ion toxicity indicates that Ni cytotoxic effects on MC3T3-E1 cells begin to be observed at fluid levels exceeding 600 ppb [44]. These data appear to explain why cell viability remained high in the hydrogels exposed to Ni metal controls, as Ni ion levels in the cell culture media hovered at the toxicity threshold. For Mn, literature indicates that cell toxicity occurs beyond approximately 550 ppb [44]. The ion release from the Mn metal controls exceeded this threshold for all time points, in agreement with the reduced cell viability observed in the hydrogels exposed to the Mn control samples. In terms of the observed toxicity of the NiMnSn alloys, the ion release data suggest that both Ni and Mn ions exceeded the toxicity thresholds by 15 to 54%. As a result, both ions likely contributed to the observed reduction in cell viability in hydrogels exposed to NiMnSn alloys.

Steps were therefore implemented to potentially reduce Ni and Mn release. In particular, the use of a PAH/PAA passivation layer applied using LbL assembly has been shown to significantly improve the corrosion resistance of aluminum [51] and to limit the transport of multivalent ions [52]. Also, based on previous work, crosslinking the PAH/PAA coating could potentially result in improved corrosion resistance relative to an uncrosslinked coating [51, 61]. Therefore, thermal PAH/PAA coating crosslinking was also investigated as a possible method to reduce Ni and Mn release and thereby

alloy cytotoxicity. The results from the cell viability and ion release studies performed on this additional set of samples are shown in **Figures 3** and **4**, respectively.

Inclusion of a PAH/PAA coating increased the cytocompatibility of NiMnSn MSMAs by approximately 36% ($p = 0.018$). This was reflected in the reduction of approximately 15% Ni and Mn ions released noted for the coated samples relative to the uncoated samples (**Figure 4**). However, crosslinking of this coating appeared to disrupt the positive effects associated with the coating itself. Specifically, the cell viability associated with alloys with cross-linked coatings could not be statistically distinguished from that of uncoated NiMnSn alloys. These results were consistent with the ion release data which showed that the reduction in ion release noted for the coated samples was largely lost following crosslinking (**Figure 4**). The impact of the coating on limiting ion release is especially apparent when Sn ion levels are examined. Specifically, Sn ion release was decreased by approximately 120% in the coated relative to the uncoated NiMnSn samples. This substantial reduction in Sn ion release is consistent with the increased size and charge of Sn ions (most commonly 4^+) relative to Mn^{2+} and Ni^{2+} ions, as PAH/PAA coatings generally have greater impact on the transport of higher valency and larger atomic radius species [52]. Based on literature, it is anticipated that increasing the number of PAH/PAA bilayers beyond the current level (10 bilayers) would result in further reductions in ion release and thereby improvements in cell viability. However, increased bilayer thickness may decrease coating compliance, resulting in delamination with cyclic MSMA deformation. Therefore, the coating thickness on shape memory

alloys must be optimized to obtain the most effective ion barrier while maintaining enough compliance to limit delamination due to martensitic transformation strain.

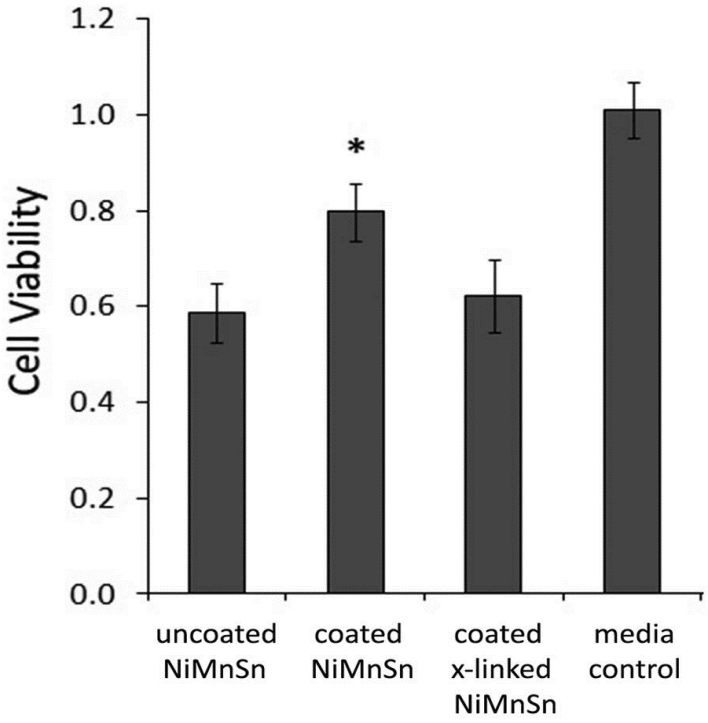

Figure 3. Cytotoxicity of uncoated NiMnSn alloys relative to NiMnSn alloys with uncrosslinked and crosslinked PAH/PAA coatings alloys as evaluated by DNA assessments. For ease of comparison, results are normalized to culture media (no metal) controls. *, significantly different from the uncoated NiMnSn alloys, $p < 0.05$.

2.4.2. Optical microscopy imaging

To determine the potential source of the unexpected increased ion release associated with coating cross-linking, optical microscopy imaging was performed on the uncoated, coated, and crosslinked-coated NiMnSn samples before and after the cell cytotoxicity experiments. **Figure 5** shows representative images of the various NiMnSn samples at day 0 and after 14 days of immersion in cell culture media. For day 0, only

one image is provided for each sample type, except for the crosslinked-coated sample. In this case, an inset image is included which shows a sample with a defect in the coating.

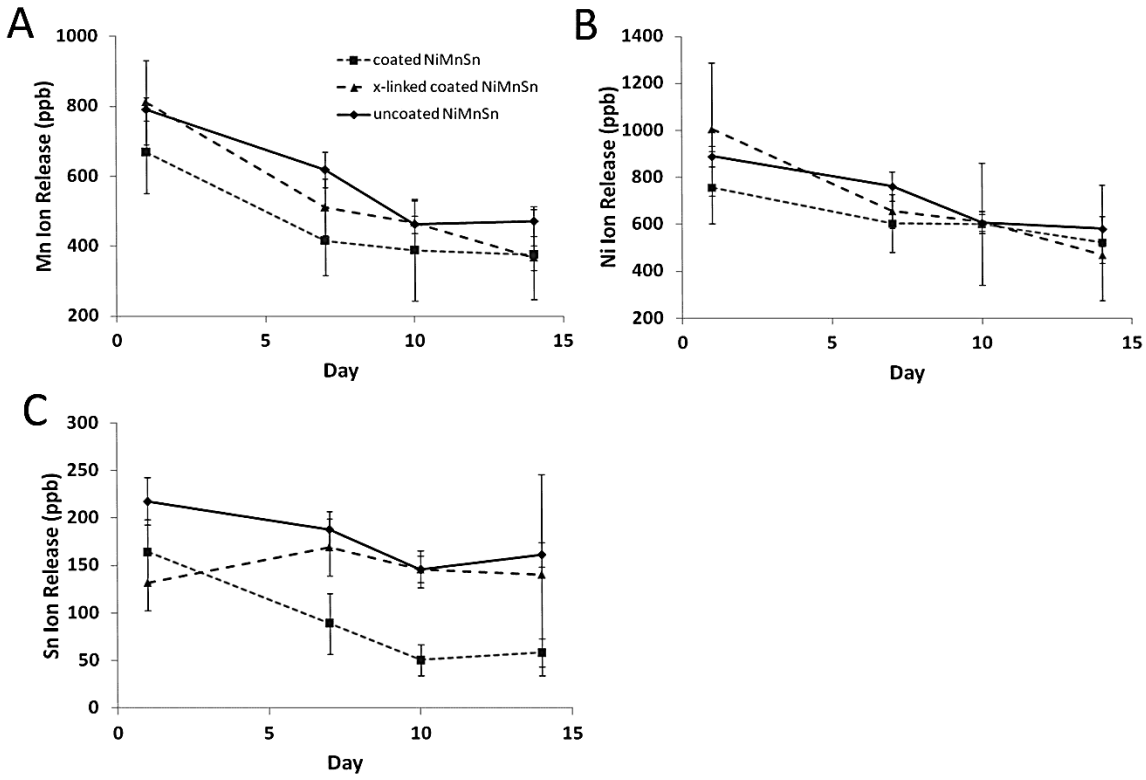

Figure 4. Mn, Ni and Sn ion release from uncoated, coated and crosslinked coated NiMnSn samples over 14 days of culture. Media surrounding each metal specimen was fully exchanged every 2 days beginning at day 1 of culture.

For the 14 day time point, two images are provided for each NiMnSn sample type - an example of a defect-free location as well as an image of a location where corrosion and/or coating degradation was observed. The ridge-like features shown in the day-14 defect-free image for the crosslinked coated samples are martensite plates resulting from the elevated temperature associated with coating crosslinking martensite transformation

temperature changes after the crosslinking heat treatment. This shows the potential for thermal crosslinking, even at 180C temperatures, to affect alloy response.

Following 14 days of culture, uncoated samples displayed relatively corrosion-free regions as well as regions with marked oxidation. This variability could have potentially resulted from localized material inhomogeneity that persisted despite the homogenization heat-treatment. On the other hand, defect locations in the coated NiMnSn samples show surface bubbles indicative of local coating delamination after 14 days immersion in cell culture media. However, the surface bubbles were generally inter-connected and there were no signs of underlying surface corrosion.

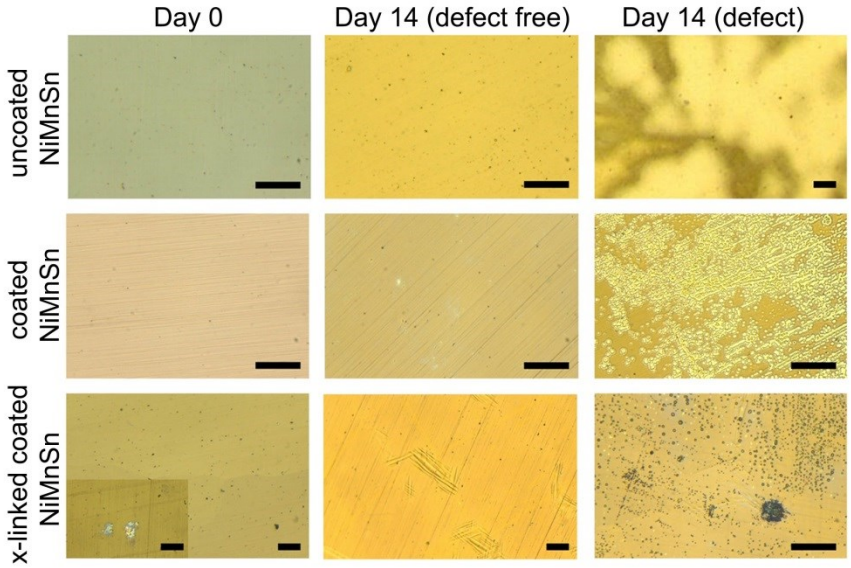

Figure 5. Representative optical microscopy images of uncoated, coated, and crosslinked (x-linked) coated samples at day 0 and after 14 days of immersion on cell culture media. Scale bars represent 50 μm. The ridge-like features shown in the day-14 defect-free image for the crosslinked coated samples are martensite plates resulting from the elevated temperature associated with coating crosslinking martensite transformation temperature changes after the crosslinking heat treatment.

Similar to the coated NiMnSn specimens, the defect regions of the crosslinked-coated samples showed delamination as indicated by the presence of bubbling of the coating surface. In this case however, the bubbles did not interconnect and corrosion discoloration was apparent on the underlying metal surface. Importantly, many of the day 14 NiMnSn specimens with crosslinked-coatings displayed larger circular regions of corrosion where coating was apparently absent. It is believed that many of these larger defect regions originated from coating shrinkage during crosslinking that resulted in localized defects (**Figure 5**, inset of day 0 crosslinked-coated samples). These results are in contrast to the improved barrier response of crosslinked PAH/PAA films in literature [61], and it is believed that improving processing parameters to prevent the observed defect formation may the overall cytocompatibility.

2.5. CONCLUSIONS

The present study was designed to evaluate the cytotoxicity of NiMnSn MSMAs as well as the impact of PAH/PAA coatings on NiMnSn cytotoxity. Based on ICP-MS measurements, Ni and Mn ion release appears to be the primary source of NiMnSn cytotoxicity in the present studies. PAH/PAA coatings appeared to improve the alloy cytocompatibility via reducing ion release. Comparison of uncrosslinked and crosslinked PAH/PAA coated specimens indicate that coating stability and integrity is critical to reducing cytotoxicity. As such, future studies will examine methods, such as chemical or UV crosslinking, to improve coating long-term integrity and surface adhesion.

CHAPTER III

INFLUENCE OF SELECT EXTRACELLULAR MATRIX PROTEINS ON MESENCHYMAL STEM CELL OSTEOGENIC COMMITMENT IN THREE-DIMENSIONAL CONTEXTS[*]

3.1. OVERVIEW

Growth factors have been shown to be powerful mediators of mesenchymal stem cell (MSC) osteogenic differentiation. However, their use in tissue engineered scaffolds not only can be costly but also can induce undesired responses in surrounding tissues. Thus, the ability to specifically promote MSC osteogenic differentiation in the absence of exogenous growth factors via the manipulation of scaffold material properties would be beneficial. The current work examines the influence of select extracellular matrix (ECM) proteins on MSC osteogenesis toward the goal of developing scaffolds with intrinsically osteoinductive properties. Fibrinogen (FG), fibronectin (FN) and laminin-1 (LN) were chosen for evaluation due to their known roles in bone morphogenesis or bone fracture healing.

These proteins were conjugated into poly(ethylene glycol) diacrylate (PEGDA) hydrogels and their effects on encapsulated 10T½ MSCs were evaluated. Specifically, following 1 week of culture, mid-term markers of various MSC lineages were examined

---

[*] Reprinted with permission from "Influence of select extracellular matrix proteins on mesenchymal stem cell osteogenic commitment in three-dimensional contexts" by Silvia Becerra-Bayona, Viviana Guiza-Arguello, Xin Qu, Dany J. Munoz-Pinto, Mariah S. Hahn, 2012, Acta Biomaterialia (2012) 4397-4404, Copyright 2012, Acta Materialia Inc. Published by Elsevier Ltd.

in order to assess the strength and specificity of the observed osteogenic responses. PEG–LN gels demonstrated increased levels of the osteogenic transcription factor osterix relative to day 0 levels. In addition, PEG–FG and PEG–LN gels were associated with increased deposition of bone ECM protein osteocalcin relative to PEG–FN gels and day 0. Importantly, the osteogenic response associated with FG and LN appeared to be specific in that markers for chondrocytic, smooth muscle cell and adipocytic lineages were not similarly elevated relative to day 0 in these gels.

3.2. INTRODUCTION

Mesenchymal stem cells (MSCs) are being increasingly recognized as a viable cell source for bone regeneration applications due to their ability to be expanded in vitro and to differentiate into a number of cell lineages. MSC differentiation is known to be influenced by a range of environmental stimuli, among the most potent of which are growth factors. However, the use of exogenous growth factors in tissue engineering scaffolds not only can be costly but also can induce undesired responses in surrounding tissues. Thus, MSC-based bone regeneration strategies would benefit from the identification of scaffold material properties which intrinsically promote osteoblast lineage progression in the absence of exogenous growth factors.

A number of two-dimensional (2-D) studies have demonstrated MSC osteogenic differentiation to be tightly regulated by cellular interactions with the surrounding extracellular matrix (ECM) [62-74]. However, comparatively, little is known regarding the effects of various ECM components in regulating MSC osteogenesis in three-

dimensional (3-D) scaffold environments [75-77]. This is significant since recent studies suggest that effects observed in two dimensions may not be indicative of the effects of the same scaffold variables in more biomimetic 3-D culture systems [78-80].Therefore, the current work focuses on elucidating the influence of select ECM constituents on MSC osteogenic differentiation in 3-D contexts.

Towards this goal, we incorporated specific ECM molecules into hydrogel scaffolds designed to have moduli within the ‘‘osteogenic’’ range identified in the 3-D human and mouse MSC studies of Huebsch et al. [81]. In selecting molecules for examination, we chose to focus on several ECM proteins associated with bone morphogenesis (fibronectin [82] and laminin-1 [83, 84]) and/or bone fracture healing (fibrinogen [85]). These proteins were then conjugated into poly(ethylene glycol) diacrylate (PEGDA) hydrogel networks. PEGDA hydrogels were selected as the base scaffold due to the broad tunability of their mechanical properties and their previous use in bone regeneration applications [2-5]. In addition, pure PEGDA hydrogels function as biological ‘‘blank slates’’ in that they do not significantly adsorb cell adhesive serum proteins and therefore do not intrinsically promote cell adhesion [6]. Thus, cell interactions with PEGDA gels are initially isolated to the proteins specifically tethered to the scaffold as well as the interactions supported by these proteins (e.g. growth factor binding).

In the present study, 10T½ MSCs were encapsulated within PEGDA hydrogels containing defined amounts of fibronectin (FN), fibrinogen (FG) or laminin-1 (LN). The levels of various markers of osteoblast, chondrocytic, smooth muscle cell and adipocytic

fates were then monitored with time in culture toward assessing the strength and specificity of observed osteogenic responses.

3.3. MATERIALS AND METHODS

3.3.1. Polymer synthesis and characterization

3.3.1.1. PEG diacrylate synthesis

PEGDA was prepared as previously described [86] by combining 0.1 mmol ml^{-1} dry PEG (10 kDa, Fluka), 0.4 mmol ml^{-1} acryloyl chloride and 0.2 mmol ml^{-1} triethylamine in anhydrous dichloromethane and stirring under argon overnight. The resulting solution was washed with 2 M K2CO3 and separated into aqueous and dichloromethane phases to remove HCl. The organic phase was subsequently dried with anhydrous MgSO4, and PEGDA was precipitated in diethyl ether, filtered and dried under vacuum. Acrylation of the PEG end hydroxyl groups was characterized by proton nuclear magnetic resonance (1H-NMR) to be ~95%.

3.3.1.2. Synthesis of acrylate-derivatized proteins

Proteins FN (human plasma, BD Biosciences), FG (human plasma, Sigma Aldrich) and LN (mouse, BD Biosciences) were lightly functionalized in their folded state by reaction with acryloyl-PEG-N-hydroxysuccinimide (ACRL-PEG-NHS, 3.4 kDa, Nektar) at a 1:2 M ratio at pH 8.5 [86]. The resulting acrylate-derivatized products were purified by dialysis against a 100 kDa membrane, lyophilized and stored at -20 °C until

use. ACRL–PEG conjugation to the target proteins was confirmed using ^{1}H-NMR. A representative ^{1}HNMR spectrum for acrylate-derivatized FG is shown in **Figure 6.**

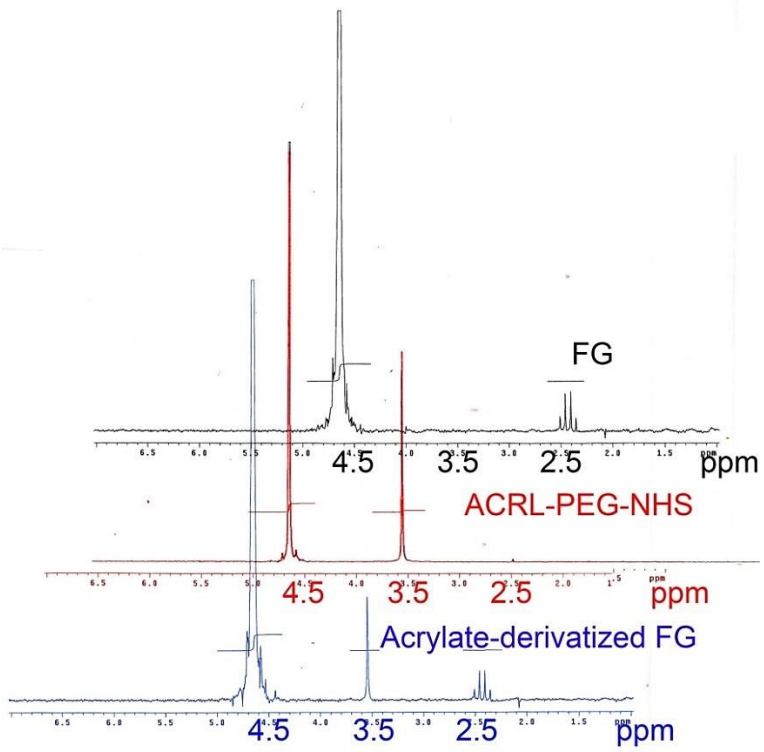

Figure 6. ^{1}HNMR spectrum of functionalized FG confirming conjugation of FG with ACRL-PEG-NHS.

To confirm the ability of the modified proteins to be incorporated within PEGDA hydrogel networks, hydrogel precursor solutions were prepared with 0.5 mg ml^{-1} protein and 100 mg ml^{-1} PEGDA (10kDa). Following the addition of 10 µl ml^{-1} of a 300 mg ml^{-1} solution of UV photoinitiator 2,2-dimethoxy-2-phenyl-acetophenone (DMAP) in N-vinylpyrrolidone (NVP), gels were polymerized by 4 min exposure to long-wave UV light (Spectroline, ~6 mWcm^{-2}, 365 nm). The gels were then immersed in PBS

overnight, after which they were transferred to a 0.12 M NaOH solution to hydrolyze the PEGDA crosslinks and release encapsulated protein. The levels of protein released were compared to the levels in the precursor solution using the CBQCA assay (Invitrogen), and the average level of protein incorporation was found to be consistent across protein types at 86.7 ± 7.2%. In addition, to assess the ability of cells to interact with proteins incorporated into the hydrogel network, 10T½ cells were seeded onto the surface of each gel formulation. Cell adhesion and spreading were confirmed for each PEG–ECM gel type (**Figure 7**).

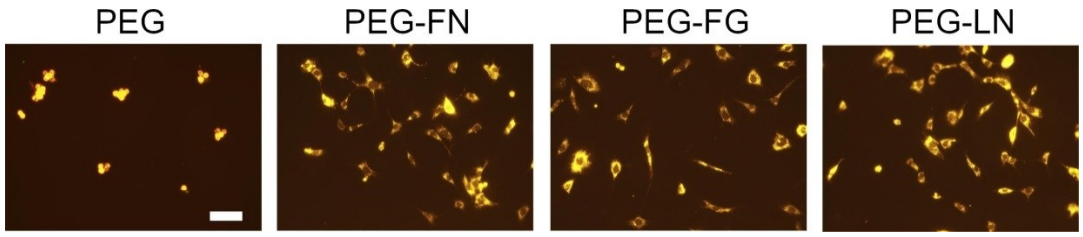

Figure 7. PEG-functionalized protein hydrogels were fabricated by combining 100 mg ml-1 PEGDA (10kDa) with photoinitiator (DMAP in NVP) and 0.5 mg ml-1 functionalized protein of FG, FN and LN. PEGDA hydrogel served as a negative control. 10T½ cells were stained with 5μM CellTracker Orange CMTMR (5-(and-6)-(((4-chloromethyl) benzoyl) amino) Tetramethylrhodamine) and seeded at a density of 6000 cells/cm2 on the surface of the hydrogels. Attached cells were allowed to spread for 3 hours and imaged by fluorescence microscopy. The scale bar applies to all images and equals 20 μm.

3.3.2. Cell culture, initial characterization and encapsulation

Cryopreserved 10T½ mouse MSCs (American Type Culture Collection; ATCC) at passage 2 were thawed and expanded in monolayer culture per ATCC protocols. Prior to encapsulation, cells were maintained at 37 °C and 5% CO_2 in Dulbecco's modified Eagle's medium (DMEM, Hyclone) supplemented with 10% heat-inactivated fetal

bovine serum (FBS, Hyclone). Cells at passage 4–6 were termed ‘‘day 0’’ and were harvested and allocated for either protein extraction or hydrogel encapsulation.

3.3.2.1. Protein extraction

Proteins were extracted from day 0 10T½ cells by the addition of Trizol (Invitrogen) per manufacture’s protocols. The resulting solutions were centrifuged, and each supernatant was mixed with chloroform (Sigma), vigorously shaken for 15 s and centrifuged. The lower protein-rich phenol–chloroform phase of each sample (n = 4) was mixed with ethanol to precipitate residual DNA. The resulting phenol–ethanol phase was transferred to a 3.4 kDa SnakeSkin dialysis membrane (Pierce). The solution was dialyzed for ~60 h at 4 °C against an aqueous solution of 0.1% sodium dodecyl sulfate (SDS), with buffer exchange every 18 h. By the end of the third 18 h dialysis period, the samples had partitioned into three phases: (1) a supernatant, (2) a globular mass and (3) a colorless, viscous liquid. The globular mass, containing the bulk of sample proteins [87], was resuspended in PBS containing 0.5% SDS and 1% Triton X-100. The isolated sample proteins were subsequently used in quantitative ELISA assays.

3.3.2.2. Cell encapsulation and culture

Hydrogels were fabricated by preparing: (1) a 20 wt.% PEGDA solution in HEPES-buffered saline (HBS) and (2) separate solutions of 1 mg ml^{-1} acrylate-derivatized FN, FG or LN in HBS. A 300 mg ml^{-1} solution of DMAP in NVP was added at 2% (v/v) to the PEGDA mixture. The PEGDA and protein solutions were then

separately sterilized by filtration, after which each protein solution was mixed with an equal volume of the 20 wt.% PEGDA solution. Harvested 10T½ cells were resuspended in the resulting precursor solutions at 1 x 10^6 cells ml^{-1}. The cell suspensions were then pipetted into molds composed of two glass plates separated by 0.5 mm polycarbonate spacers and polymerized by 4 min exposure to long-wave UV light (Spectroline, ~6mWcm^{-2}, 365 nm). A set of the resulting hydrogels were harvested for ‘‘day 0’’ analyses as described in the following section. The remaining hydrogel slabs were transferred to Omnitrays (Nunc) fitted with four sterile polycarbonate bars to simultaneously prevent gel flotation and prevent gel contact with the tray bottom. Hydrogels were immersed in DMEM supplemented with 10% FBS, 100 U ml^{-1} penicillin and 100 mg l^{-1} streptomycin. Gels were maintained at 37 °C and 5% CO_2, with media changes every 2 days.

3.3.3. Day 0 hydrogel characterization

3.3.3.1. Average mesh size

PEGDA hydrogel mesh structure cannot be visualized using standard techniques such as scanning electron microscopy. In the present study, average hydrogel mesh size was therefore characterized via a series of dextran diffusion experiments based on an adaptation of the methodology of Watkins and Anseth [88]. In brief, samples were collected from the freshly prepared PEG– ECM hydrogels and allowed to swell overnight at 37 °C in PBS containing 0.05% azide (PBS-azide). Eight-millimeter-diameter discs were then harvested from each gel formulation, and solutions containing

0.05 mg ml^{-1} fluorescently labeled dextran (10 kDa, Invitrogen) in PBS-azide were added at 1 ml per hydrogel disc. Dextran solutions were allowed to diffuse into the hydrogels for 24 h at 37 °C. Each gel disc was then gently blotted and transferred to 1 ml fresh PBS-azide. Dextran that had penetrated into the hydrogels was then permitted to diffuse out into the surrounding solution at 37 °C. After 24 h, the fluorescence of the PBS-azide solution surrounding each disc was measured at ex/em 488/532. Dextran standard curves were used to convert each fluorescence signal to a concentration. For each hydrogel, the measured dextran concentration was divided by gel weight [89]. The resulting value served as a quantitative indicator of hydrogel permissivity.

3.3.3.2. Hydrogel mechanical properties

Samples were collected from each freshly prepared hydrogel formulation and allowed to swell overnight in PBS-azide. Eight mm discs (n = 4 per formulation) were then cored from each gel sample and mechanically tested under unconfined compression using a DMA 800 (TA Instruments). Following application of a 0.01 N preload, each disc was subjected to compression at a rate of 0.1 mm min^{-1}. The compressive modulus of each hydrogel was extracted from the resulting stress–strain data over a 10–25% strain range.

3.3.3.3. Cell density

Samples (n = 4) were collected from each freshly prepared hydrogel formulation following 24 h immersion in culture media. Hydrogel samples were digested for 72 h at

37 °C in 1 ml of 0.12 M NaOH per 0.2 g hydrogel wet weight [90, 91]. Aliquots of the hydrolyzed samples were neutralized, and their DNA content determined using the Invitrogen PicoGreen assay [92]. DNA measures were translated to cell number using a conversion factor of 6.6 pg DNA per cell [93]. Calf thymus DNA (Sigma) subjected to the same association with PEGDA and to the same digestion conditions as the samples served as a standard.

3.3.4. Endpoint analyses

At day 7 of culture, samples were harvested from each hydrogel formulation for mechanical, mesh size, DNA, ELISA and histological analyses. Samples collected for histological analyses (n = 4–8 per formulation) were fixed in 10% formalin for 30 min and embedded in Tissue-Tek freezing medium. Samples harvested for mechanical (n = 4 per formulation), mesh size (n = 4 per formulation) and DNA (n = 4 per formulation) assessments were evaluated according to the same protocols as the day 0 specimens. Similarly, samples harvested for ELISA analyses (n = 6–9 per formulation) were homogenized in Trizol using a Bead-Beater homogenizer (Biospec), after which sample proteins were isolated as described for day 0 specimens.

3.3.4.1. ELISA analyses

Proteins extracted from the day 0 cells and the day 7 constructs were evaluated for various lineage markers and integrin alpha subunits via competitive ELISAs. For each antibody examined, high binding EIA 96-well plates (Costar) were coated

overnight at 4 °C with appropriate competitive peptide. The concentration of applied competitive peptide was 200 ng per well, except for b-actin (50 ng per well). The coated wells were then blocked with BSA and rinsed with PBS. Aliquots of each sample were incubated with primary antibody for 1 h, after which the sample–antibody mixtures were applied to coated wells for 1 h. Standard curves were similarly prepared by incubating primary antibody with varying levels of competitive peptide for 1 h, followed by solution application to coated wells. For both samples and standards, primary antibody which had bound to the coated wells was detected using an appropriate HRP-conjugated secondary antibody (Jackson Immunoresearch), followed by the application of 2,20-azino-bis(3-ethylbenzthiazoline-6-sulphonic acid) (Sigma) and monitoring of absorbance at 410 nm. Each target protein was analyzed in duplicate for each sample (n = 6–9 per day 7 gel type; n = 4 for day 0) and normalized to the housekeeping protein b-actin.

3.3.4.2. Histological analyses

Bone ECM deposition (osteopontin and osteocalcin) was further analyzed using standard immunohistochemical techniques. In brief, 35 μm sections were cut from each embedded histological sample (n = 4–8 per formulation) using a cryomicrotome. Rehydrated sections were blocked for peroxidase for 30 min followed by 30 min exposure to Terminator (Biocare Medical). Primary antibodies for osteopontin and osteocalcin were diluted in PBS containing 3% BSA and then applied to the sections for 1 h. Bound primary antibody was detected using HRP-conjugated secondary antibody (Jackson Immunoresearch) followed by the application of chromogens AEC (LabVision)

or DAB (Biocare Medical). For the detection of intracellular differentiation markers (myocardin and PPARγ), rehydrated sections were permeabilized (10 mM HEPES, pH 6.8, 100 mM NaCl, 3 mM $MgCl_2$, 300 mM sucrose, 0.5% Triton X-100) for 30 min prior to Terminator application.

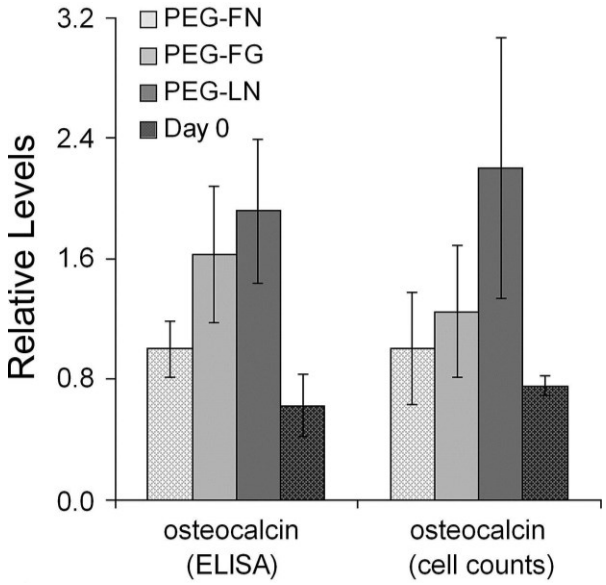

Figure 8. Comparison of osteocalcin measures by ELISA and cell counting assessments. For ELISA assays, 6-9 samples per formulation were analyzed. For cell counts, sections from 4 separate discs of each formulation were evaluated. The degree of correlation between the two assessment techniques was 98.5% by Pearson's correlation coefficient method

Stained sections were imaged using a Zeiss Axiovert microscope, and cell counts were carried out to semi-quantitatively evaluate immunostaining results for intracellular markers myocardin and PPARγ. These counting assessments were conducted according to established methods [2, 94, 95] on sections from each sample (n = 4–8 per gel formulation). For each cell, *i*, in a given section, a single observer blinded to outcome assigned a staining intensity, d_i, on a scale of 0–3 (0 = ''no staining'' and 3 = ''highest

intensity among all formulations for that antibody''). The cumulative staining intensity, *d*, for a given antibody in a particular section was calculated using the following equation: $d = (\sum d_i)/(\text{total cell number})$. In addition, since deposited ECM remained localized around the parent cells in each hydrogel formulation, as is characteristic for PEGDA gels [96], the relative levels of osteocalcin and osteopontin among hydrogel formulations were also evaluated by cell counts per the above procedure. Osteocalcin counts were used to internally validate the counting approach by direct comparison with corresponding quantitative ELISA data (**Figure 8**). The degree of correlation between the two assessment techniques was 98.9% by Pearson's correlation coefficient method.

3.3.5. Statistical analyses

Data are reported as mean ± standard deviation. Comparison of sample means was performed by ANOVA followed by Tukey's post hoc test (SPSS software), $p < 0.05$.

3.4. RESULTS

3.4.1. Hydrogel material properties and cell density

A range of scaffold properties, including modulus, permeability and degradation rate, have been found to impact MSC lineage progression. Therefore, in order to attribute differences in 10T½ cell behavior across hydrogel formulations specifically to initial differences in gel protein composition, it was important that the remaining hydrogel material properties could be considered consistent across gels. Hydrogels

formed from pure PEGDA degrade slowly (over a period of 1–2 years) and resist cell-mediated gel contraction, ensuring consistent bulk gel properties over a broad time range [91, 92, 97-99]. In the present study, a 200:1 weight ratio of PEGDA to protein was therefore selected to ensure that the network properties of the resulting gels would be dominated by PEGDA. To confirm this, the modulus, mesh size, thickness and mass of the PEG–ECM hydrogels were characterized both at day 0 and at day 7.

As shown in **Table 1**, the initial elastic moduli of the PEG–FG, PEG–FN and PEG–LN gels were similar at ~33 kPa. Importantly, each of these initial moduli were within the osteogenic range identified by the 3-D studies of Huebsch et al. [81]. To assess degradation and cell-mediated contraction, hydrogel modulus and thickness were evaluated across time in culture. Comparison of initial and endpoint mechanical data indicated that, although the modulus decreased by ~15% over the 7 day culture time for each gel formulation, hydrogel modulus remained consistent across formulations (**Table 1**). Similarly, average mesh size was consistent across hydrogels at both day 0 and day 7 (**Table 1**).

Table 1. Comparison of the average modulus and mesh size of 8 mm discs of each PEG–ECM hydrogel formulation with time in culture.[a]

Gel type	Modulus (kPa)		Mesh size (μg dextran/g-gel)	
	Day 0	Day 7	Day 0	Day 7
PEG-FN	33.3 ± 0.7	29.2± 0.8*	11.8 ± 0.3	12.4± 0.3
PEG-FG	33.9 ± 1.9	29.9± 1.5*	11.4 ± 0.3	11.7± 0.2
PEG-LN	33.7 ± 2.0	28.7± 1.2*	11.6 ± 0.3	11.8± 0.6

[a] Property results represent an average of n = 4 samples for each PEG-ECM formulation
* Significantly different from the corresponding day 0 value, $p < 0.05$.

The initial and endpoint thickness data for 8 mm gel discs indicated a negligible alteration in gel volume with time. In addition, net cell proliferation and loss were examined for each PEG–ECM hydrogel over the 7 day culture period. The cell density in each PEG–ECM hydrogel following 7 days of culture was between 78 and 86% of the initial seeding density (**Table 2**), consistent with PEG hydrogel literature [4, 64, 70, 76, 100-102]. Combined, the above data indicate that: (1) each hydrogel formulation maintained an osteogenic modulus throughout the study [81] and (2) differences in cell responses among formulations can be attributed to differences in the initial proteins tethered to the gel network, their interactions with other molecules and subsequent neo-matrix deposition.

Table 2.Comparison of the average thickness, mass, and cell density in discs of each PEG–ECM hydrogel formulation with time in culture.[a]

Gel type	Thickness (mm)		Mass of 8mm discs (mg)		Cell density (x10^6)	
	Day 0	Day 7	Day 0	Day 7	Day 0	Day 7
PEG-FN	0.55 ± 0.01	0.56± 0.01	29.1 ± 0.2	29.5± 0.2	1.01± 0.06	0.88± 0.08*
PEG-FG	0.55 ± 0.01	0.56± 0.01	29.2 ± 0.2	29.4± 0.5	0.96± 0.05	0.72± 0.02*
PEG-LN	0.54 ± 0.01	0.56± 0.01	29.2 ± 0.4	29.3± 0.3	1.01± 0.06	0.82± 0.02*

[a] Results represent an average of n = 4 samples for each PEG–ECM formulation.
* Significantly different from the corresponding day 0 value, $p < 0.05$.

3.4.2. Cell differentiation

Following 7 days of culture, cell differentiation was examined by quantitative ELISA or by cell counts (as validated in **Figure 8**). As shown in **Figure 9**, day 7 levels of various osteogenic markers indicated significant differences relative to day 0 and/or

among hydrogel formulations. Specifically, cells in PEG–LN gels expressed significantly higher levels of the osteogenic transcription factor osterix than day 0 cells ($p = 0.032$), while osterix expression in PEG–FN gels could not be distinguished from day 0 levels. In addition, PEG–LN gels retained day 0 osteopontin expression levels, whereas osteopontin levels in day 7 PEG–FN gels had fallen to approximately half of day 0 levels ($p = 0.005$). Similarly, day 7 PEG–FN gels contained significantly lower levels of the bone ECM protein osteocalcin relative to PEG–FG ($p = 0.042$) and PEG–LN ($p = 0.002$) gels, whereas PEG–FG and PEG–LN gels contained 2.4- and 2.9-fold greater osteocalcin levels than day 0 ($p = 0.004$ and $p < 0.001$, respectively).

To assess the specificity of the osteogenic response associated with the PEG–FG and PEG–LN gels, mid-term markers of chondrogenesis, smooth muscle progression and adipogenesis were evaluated (**Figure 10**). Day 7 expression of smooth muscle transcription factor myocardin was similar to day 0 levels and across hydrogel formulations. In addition, day 7 levels of SM22α, a cytoskeletal protein associated with smooth muscle differentiation, could also not be distinguished among gel formulations or from day 0 levels. PPARγ expression was similar to day 0 levels across the day 7 gels, and the day 7 levels of the adipocyte intracellular protein A-FABP were statistically indistinguishable from day 0 levels and among formulations. Furthermore, day 7 expression of chondrogenic transcription factor sox9 did not vary significantly with gel formulation or relative to day 0, and day 7 levels of the cartilage-associated ECM protein collagen II could also not be distinguished among the PEG–ECM gels or relative to day

0. Representative immunostaining images for proteins evaluated by cell counts (myocardin, PPARγ, and osteopontin) are given in **Figure 11**.

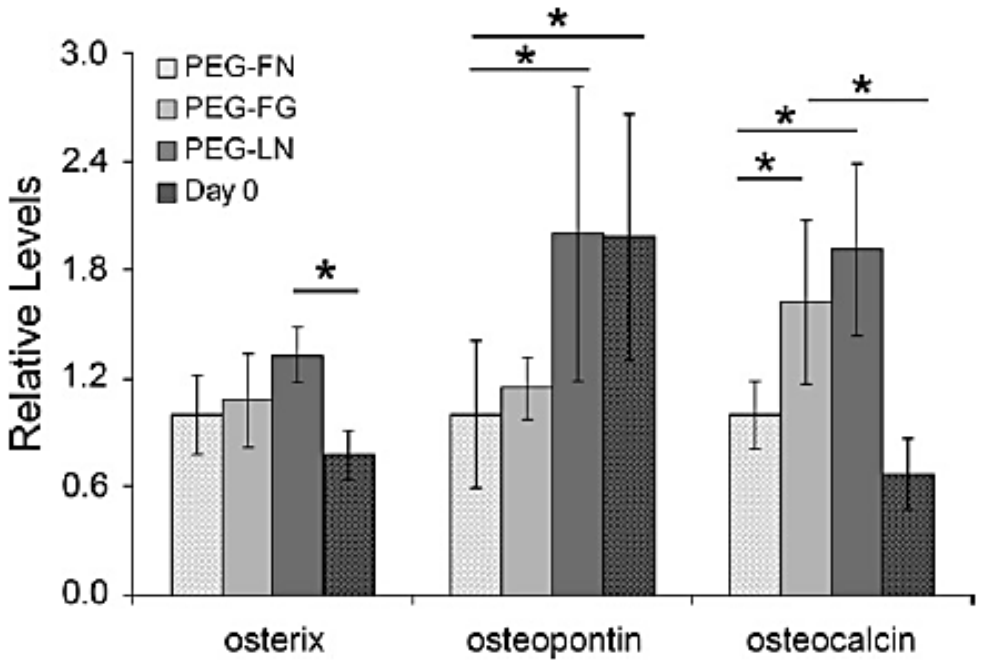

Figure 9. Expression of osteogenic markers osterix, osteopontin and osteocalin by ELISA (osterix and osteocalcin) and cells counts (osteopontin). For ELISA assays, six samples per day 7 formulation were analyzed. The day 0 ELISA sample number was n = 4. For cell counts, sections from 4-8 separate samples of each formulation were evaluated. Validation of the cell counting assessment method is given in Fig. 3. For the purpose of comparison, ELISA and cell count measures for each protein have been normalized to the corresponding measure for PEG-FN gels. *indicates a significant difference, $p < 0.05$

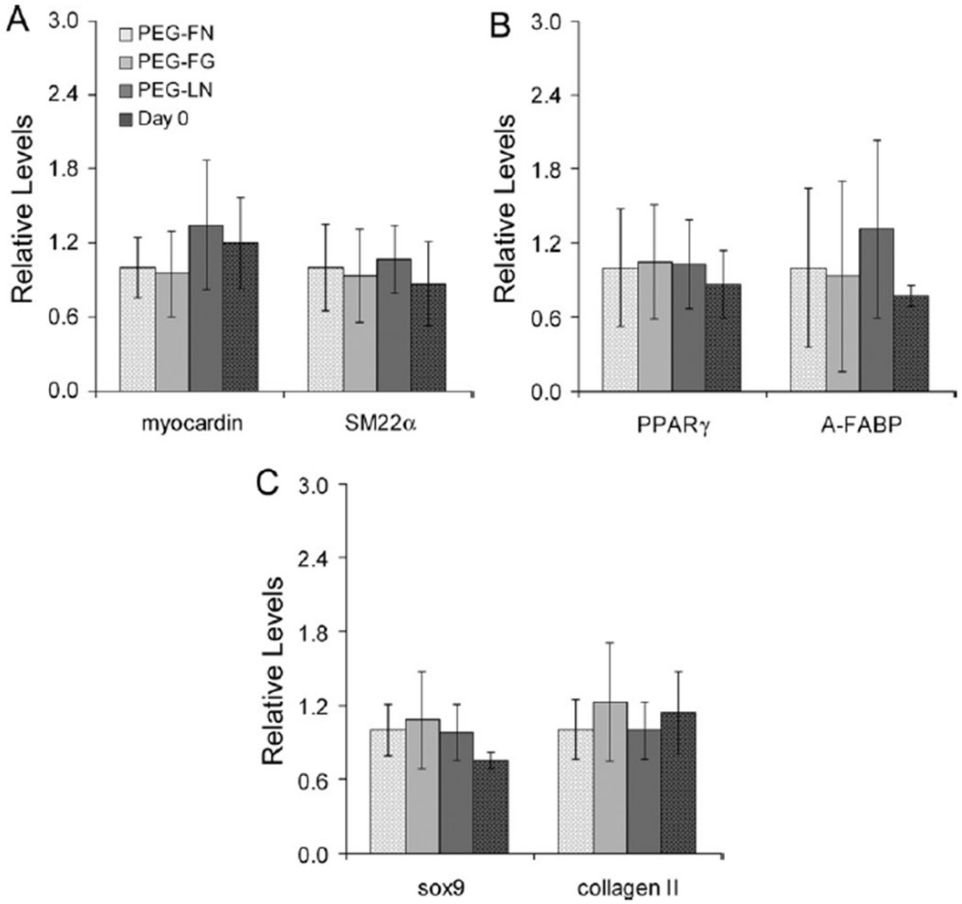

Figure 10. (A) Expression of myocardin and SM22α, as assessed by cell counting and ELISA methods, respectively. (B) Expression of PPARγ and A-FABP, as assessed by cell counting and ELISA methods, respectively. (C) Expression of sox9 and collagen II by ELISA. For ELISA assays, 6–9 samples per day 7 formulation were analyzed. The day 0 ELISA sample number was n = 4. For cell counts, sections from four separate samples of each formulation were evaluated. For the purpose of comparison, ELISA and cell count measures for each protein have been normalized to the corresponding measure for PEG–FN gels.

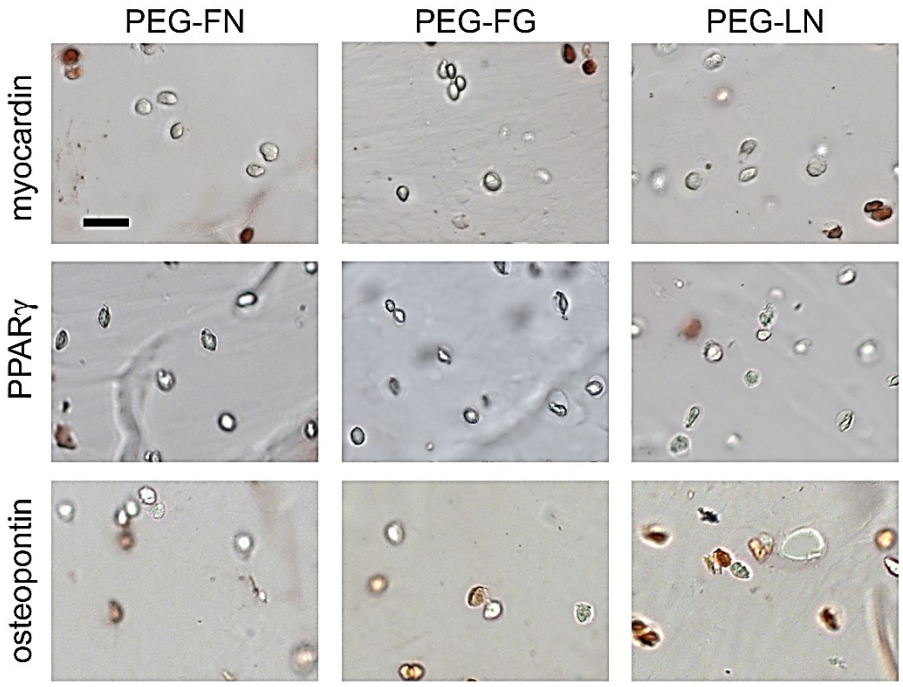

Figure 11. Representative images of day 7 immunostaining for myocardin, PPARγ and osteopontin. Positive staining is indicated by brown (PPARγ and osteopontin) or red (myocardin) coloration. Scale bar = 40 μm and applies to all images.

3.5 DISCUSSION

The aim of the present work was to compare the osteoinductivity of select ECM components in defined 3-D environments toward the improved design of osteogenic scaffolds. To avoid the use of exogenous growth factors, these ECM components were examined within the context of scaffolds with osteogenic moduli (~30 kPa) [81]. Present data indicated that both FG and LN enhanced the osteogenic response of encapsulated 10T½ cells. Specifically, osteocalcin levels in day 7 PEG–FG and PEG–LN gels were ~2.4- and 2.9-fold greater, respectively, than day 0 levels. In addition, expression of osterix, an osteoblast-specific transcription factor required for osteogenesis, was significantly elevated in day 7 PEG–LN gels relative to day 0 levels. In contrast, the day

7 levels of markers for adipogenesis, chondrogenesis and smooth muscle lineage progression were not significantly different among formulations or relative to day 0, indicating that the osteogenic response associated with the PEG–FG and PEG–LN gels was specific.

The present results are consistent with previous 2-D studies demonstrating LN to support higher active levels of the osteogenic transcription factor Cbfα1 than FN over a 5 day culture time frame [72]. In addition, a study by Salaszynk et al. indicated that, in the absence of osteogenic media supplements, FN did not support human MSC matrix mineralization, in contrast to collagen I and vitronectin [103]. Indeed, they found little role for FN in stimulating osteogenic differentiation [65], beyond activation of alkaline phosphatase [103]. Similarly, Benoit et al. found that FN increased alkaline phosphatase production, but not osteopontin gene expression [76]. Although fibrin glue has been used extensively in bone tissue engineering [85, 104-113], literature presents conflicting reports regarding the osteoinductivity of fibrinogen. Specifically, while several studies have suggested that fibrin sealants promote osteogenesis [107, 109-111], other studies have reported negative effects when fibrin sealants were combined with coral granules [112, 113] and poly(lactide-co-glycolic acid) scaffolds [104]. These conflicting results may arise, in part, from differences in the material properties of the various fibrin-containing scaffolds assayed. In the present study, we tightly controlled initial scaffold material properties as well as the temporal evolution of those properties in order to isolate the osteoinductive effect of FG from other matrix properties.

Moreover, since integrin-associated signaling has been demonstrated to play a key role in MSC osteogenic lineage progression [62-64, 69, 70, 73, 103], further studies conducted in our lab indicated that initial cell adhesion to functionalized FG was mediated by α_v and α_5 integrin subunits. In contrast, cell binding to FN was predominantly mediated by α_2, α_v and α_5 integrin subunits, whereas LN interacted with α_1, α_v, α_5 and α_6 integrin subunits. Collectively, these results suggested that α_1, α_2, and α_6 integrin mediated adhesion might have strongly influenced the observed differentiation results. Nonetheless, osteogenesis represents a complex set of processes that are mediated by a number of factors. The interplay between these factors and the precise sequences leading to osteogenic commitment are not fully understood, and the present study examined only a limited subset of the interactions and a limited panel of the markers that characterize osteogenesis. In addition, the present study was conducted using cells derived from the mouse embryonic mesoderm. Although these cells demonstrate multipotency, their responses may not be indicative of the behavior of adult human mesenchymal stem cells.

Despite these limitations, the cumulative ECM and phenotypic data indicate that LN may be the most appropriate of the biomolecules examined for promoting specific osteogenic differentiation within the context of scaffolds with osteoinductive moduli. Future studies will focus on exploring a broader range of time points and ECM protein concentrations as well as on examining potential synergy between various ECM components.

CHAPTER IV

BIOMIMETIC HYDROGELS FOR THE FABRICATION OF TISSUE-ENGINEERED VASCULARIZED BONE CONSTRUCTS*

4.1. OVERVIEW

The results from the studies previously described in chapter III suggested that α1 and α2 integrin cell adhesion is probably involved in mesenchymal stem cell osteogenesis. Nonetheless, in this particular case, the complexity of the interplay among the multiple signals provided to the cells made it difficult to determine whether α1 and α2 integrin adhesion was responsible for the differentiation profiles observed. The ideal system for evaluating the effect of a specific signal on cell behavior would allow the incorporation of the desired signaling in an appropriate three-dimensional (3D) protein structure without the additional signals associated with the biopolymer. In the present study, we employed a novel biomaterial platform based on a collagen-mimetic protein derived from group A Streptococcus, Scl2.28, which maintains the native triple helical structure of native collagen and allows the incorporation of desired integrin-binding motifs. We have engineered two Scl2 "daughters",Scl2-2 (or DC2) and Scl2-3 (or DC3),

---

* Portion of this chapter was reprinted with permission from "Bioactive hydrogels based on Designer Collagens" by Cosgriff-Hernandez E, Hahn MS, Russell B, Wilems T, Munoz-Pinto D, Browning MB, Rivera J, Höök M, 2010, Acta Biomaterialia (2009) 3969-3977, Copyright 2010, Acta Materialia Inc. Published by Elsevier Ltd.
Portion of this chapter was reprinted with permission from "Multilayer Vascular Grafts Based on Collagen-Mimetic Hydrogels" by M.B. Browning, D. Dempsey, V. Guiza, J. Rivera, M. Höök, B. Russell, F. Clubb, M. Miller, T. Fossum, M. Hahn, E. Cosgriff-Hernandez, 2011, Acta Biomaterialia (2012), 8, 1010-1021 (2012), Copyright 2011, Acta Materialia Inc. Published by Elsevier Ltd.

which incorporate α1β1 and/or α2β1 integrin-binding motifs based on the collagen sequences GF/LOGER [7, 8]. DC2 and DC3 were covalently crosslinked to poly(ethylene glycol) diacrylate (PEGDA) through established polymer chemistry in order to generate hybrid biosynthetic hydrogels.

Our lab has previously shown that these hybrid PEGDA-DC gels support osteogenesis and therefore, could be potentially used in biomedical applications as osteoinductive scaffolds. Nonetheless, in the context of orthopedic applications, bone replacement materials are more effective if they also support capillary formation in addition to osteogenesis [9, 10]. Thus, a bone regeneration scaffold must be able to support endothelial cell adhesion and migration. In native vessels, collagen-based α1β1 and α2β1 integrin binding motifs have been shown to modulate endothelial cell (EC) adhesion and phenotype [114]. Therefore, given that DC2 and DC3 incorporate α1β1 and/or α2β1 integrin-binding motifs, the PEGDA-DC hybrid systems proposed in this work should have the ability to promote EC adhesion and spreading. The aim of this study was to test the ability of PEGDA-DC hydrogels to support EC adhesion, spreading and migration. The results from the adhesion and migration studies indicate that this novel hydrogel platform has the potential to improve on current options for the fabrication of highly functional tissue-engineered vascularized bone constructs.

4.2. INTRODUCTION

The results from the studies previously described in chapter III suggested that α1 and α2 integrin cell adhesion is probably involved in mesenchymal stem cell

osteogenesis. Nonetheless, in this particular case, the complexity of the interplay among the multiple signals provided to the cells made it difficult to determine whether α1 and α2 integrin adhesion was responsible for the differentiation profiles observed. The ideal system for evaluating the effect of a specific signal on cell behavior would allow the incorporation of the desired signaling in an appropriate three-dimensional (3D) protein structure without the additional signals associated with the biopolymer. In the face of this challenge, we have recently developed a novel biomaterial platform based on a collagen-mimetic protein derived from group A Streptococcus, Scl2.28. Scl2.28 or the "parent" DC (also known as DC1) maintains the native triple helical structure of native collagen but contains no known cell signaling sequences [115, 116]. Thus, DC1 provides a "blank-slate" into which desired collagen-based, cell adhesion sequences can be programmed into specific regions of the triple helix via site-directed mutagenesis of the gene encoding for DC1 (Scl2.28) while maintaining the triple helical context natively associated with these motifs [117]. In conjunction with Dr. Russell of the Höök lab at Texas A&M Health Science Center, we have engineered two "daughter" DCs, Scl2-2 (or DC2) and Scl2-3 (or DC3), which incorporate α1β1 and/or α2β1 integrin-binding motifs based on the collagen sequences GF/LOGER [7, 8]. DC2 and DC3 were covalently crosslinked to poly(ethylene glycol) diacrylate (PEGDA) through established polymer chemistry in order to generate hybrid biosynthetic hydrogels. PEGDA was selected as the synthetic component of these hybrid hydrogels due to the fact that pure PEGDA gels intrinsically resist protein adsorption and cell adhesion [6, 117, 118], a feature that allowed to focus on the bioactive signals introduced into the hydrogels by the DCs. In

addition, PEGDA gels have been previously used in bone regeneration applications because of the broad tunability of their mechanical properties [2-5].

Our lab has previously shown that these hybrid PEGDA-DC gels support osteogenesis. Specifically, following two weeks of culture, calcium deposition was significantly enhanced in human mesenchymal stem cells (hMSCs) encapsulated in PEGDA-DC2 gels relative to PEGDA-DC1 and PEGDA-DC3 samples. In addition to this, western blot assays revealed a significant increase in osterix and osteopontin expression in PEGDA-DC3 gels by ~ 1.4- and 1.2-fold, respectively, relative to PEG-DC2 gels. Based on these promising results, our novel PEGDA-DC hydrogels could be potentially used in biomedical applications as osteoinductive scaffolds. Nonetheless, in the context of orthopedic applications, in vivo and in vitro studies have demonstrated that bone replacement materials are more effective if they also support capillary formation in addition to osteogenesis [9, 10]. In this way, the presence of endothelial cells may accelerate the defect healing process by improving cell nutrition in the scaffolds as well as in the defect site. Thus, a bone regeneration scaffold must be able to support endothelial cell adhesion and migration. In native vessels, collagen-based α1β1 and α2β1 integrin binding motifs have been shown to modulate endothelial cell (EC) adhesion and phenotype [114]. Therefore, given that DC2 and DC3 incorporate α1β1 and/or α2β1 integrin-binding motifs, the PEGDA-DC hybrid systems proposed in this work should have the ability to promote EC adhesion and spreading. However, this must be confirmed in our PEGDA-DC system.

The aim of this study was to test the ability of PEGDA-DC hydrogels to support EC adhesion, spreading and migration. EC adhesion studies confirmed cell-specific adhesion due to selective integrin binding to the two receptor binding motifs investigated. On the other hand, evaluation of EC migration speed demonstrated that PEGDA-DC hydrogels promoted higher migration speeds than PEGDA-collagen analogs and that migration speed was readily tuned by altering protein concentration. Collectively, these results indicate that this novel hydrogel platform has the potential to improve on current options for the fabrication of highly functional tissue-engineered vascularized bone constructs.

4.3. MATERIALS AND METHODS

4.3.1. Scl2 functionalization

The Scl2.28 sequence was amplified and purified as previously described [119]. Scl2-1 (or DC1) served as a negative control with no binding sites for α1β1 or α2β1. Scl2-2 (or DC2) is a variant of this protein containing the sequence GFPGER that was generated by site directed mutagenesis as previously described [120]. Scl2 proteins and a rat tail collagen type I control were functionalized with photoreactive crosslink sites according to a protocol adapted from Sebra et al [120]. Scl2 proteins include ~9% lysine groups that allow for bioconjugation through the established NHS-lysine Ɛ-amino group reaction. Briefly, the proteins were reacted with acrylate-PEG-N-hydroxysuccinimide (Acr-PEG-NHS, MW 3500, Jenkem Technologies USA, Allen, TX) in 50 mM sodium bicarbonate buffer (pH 8.5). The Acr-PEG-NHS:NH2 molar ratio was 1:1, and the

reaction was allowed to proceed with stirring for 24 hours at room temperature. Acidic byproducts were removed via dialysis against 0.1M hydrochloric acid for 24 hours, and further purification was carried out with dialysis against deionized water for 24 hours (MWCO = 20,000). Functionalization of the modified proteins was confirmed with Fourier transform infrared (FTIR) spectroscopy and sodium dodecyl sulfate poly-acrylamide gel electrophoresis (SDS-PAGE), as previously shown [119].

4.3.2. Preparation of bioactive PEGDA-Scl2 hydrogels

PEGDA was synthesized according to a method adapted from Hahn, et al . Briefly, 4 molar equivalents of acryloyl chloride were added dropwise to a solution of PEG (3.4 kDa or 6kDa; 1 molar equivalent) and triethylamine (2 molar equivalents) in anhydrous dichloromethane (DCM) under nitrogen. After the addition was complete, the reaction was stirred for 24 hours. The resulting solution was washed with 2M potassium bicarbonate (8 molar equivalents) and dried with anhydrous sodium sulfate. The product was precipitated in cold diethyl ether, filtered, and dried under vacuum. FTIR spectroscopy and proton nuclear magnetic resonance (1H-NMR) spectroscopy were used to confirm functionalization of PEGDA. Control and functionalized polymers were solution cast directly onto KBr pellets to acquire transmission FTIR spectra using a Bruker TENSOR 27 spectrometer. Successful acrylation was indicated by an ester peak at 1730 cm-1 and loss of the hydroxyl peak at 3300 cm-1 in the spectra. Proton NMR spectra of control and functionalized polymers were recorded on Mercury 300 MHz spectrometer using a TMS/solvent signal as an internal reference. All syntheses resulted

in percent conversions of hydroxyl to acrylate endgroups of greater than 85%. 1H-NMR (CDCl3): 3.6 ppm (m, -OCH2CH2-), 4.3 ppm (t, -CH2OCO-) 5.8 ppm (dd, -CH=CH2), 6.1 and 6.4 ppm (dd, -CH=CH2).

PEGDA, PEGDA-Scl2, and PEGDA-collagen hydrogels were prepared by dissolving PEGDA (10 or 20 wt%) and functionalized Scl2 or collagen (4, 6, 9, 12 or 15 mg ml-1) in deionized water. A photointiator solution (1 mg Irgacure 2959 per 0.1 ml 70% ethanol) was added at 1% volume of precursor solution. Solutions were pipetted into a mold and crosslinked by 6 min exposure to long wave UV light (Intelli Ray Shuttered UV Flood Light, Integrated Dispensing Solutions, Inc., 365 nm, 4 mW/cm2).

4.3.3. Endothelial cell adhesion

For cell adhesion studies, microtiter plates were coated with functionalized and unmodified Scl2-1, Scl2-2, and Scl2-3. Rat tail collagen I coated wells served as positive controls. Microtiter wells were coated with 1 μg per well of Scl2 1, Scl2-2, Scl2-3, or rat tail derived collagen type I (Cultrex R&D) in PBS overnight at 4°C. The Scl2 protein solutions were filter-sterilized using a 0.22 μm PDVF membrane (Millipore) prior to application to the microtiter plate. For each Scl2 protein, 15 wells (3 wells per cell type examined) were coated. After blocking with PBS containing 1% BSA for 1 h, the wells were rinsed extensively with PBS and cells were seeded onto the coated surfaces at 20000 cells/cm2.

Prior to seeding, cells were adapted to serum free media (DMEM containing 1mM CaCl2 and 1mM MgCl2) for 3 h, after which cells were harvested by brief

exposure to 0.125% trypsin (Mediatech) and resuspended in serum free media supplemented with 0.2% BSA. Following 3 h exposure to the coated surfaces at 37 °C / 5% CO2, cells were fixed with 4 % paraformaldehyde and stained with rhodamine phalloidin (Invitrogen) and SybrGreen (Invitrogen). Rhodamine- labeled phalloidin in combination with SybrGreen were chosen as cell markers because phalloidin binds to F-actin, which is present in abundance in cell cytoplasm, and SybrGreen binds DNA, which indicates the location of the nucleus of each cell. Representative fluorescence images were obtained using a Zeiss Axiovert microscope.

4.3.4. Quantitative analysis of cell adhesion and spreading

Fluorescence images (3 images per sample, 3 samples per protein) of SybrGreen and rhodamine phalloidin stained cells seeded onto coated tissue culture plastic were utilized to quantify the extent of cell adhesion and spreading. The number of cell nuclei per image was used as a quantitative assessment of cell adhesion on each test surface and was assessed by two independent observers. Average cell spreading, or cell area, was quantified by applying the Photoshop "magic wand" tool to the image background and adjusting the tool tolerance so that all extracellular regions were selected. The histogram function was then utilized to evaluate the extracellular pixels. The average pixels per cell (Acell) for that image was then quantified as follows: Acell = (total image pixels – extracellular pixels)/(total image nuclei). Pixels were then converted to microns using known objective scaling. Data are reported as mean ± standard error of the mean

4.3.5. Endothelial cell migration

For the PEGDA-Scl2 hydrogels to support vascularization, they must support EC adhesion and enable sufficient EC migration. To analyze EC migration on PEGDA-Scl2 hydrogels, sterile filtered PEGDA-Scl2-2 (10 wt% PEGDA, 3.4 kDa, 6 or 12 mg protein/ml) and PEGDA-collagen (10 wt% PEGDA, 3.4 kDa, 2 or 4 mg protein/ml) hydrogels were prepared between glass plates separated by 0.5 mm spacers. The resulting hydrogels were immersed in PBS for 24 h, after which a set of 2.54 cm punches were collected from the swollen gels.

Bovine aortic endothelial cells (BAECs) were harvested and seeded onto the hydrogels at 10,000 cells cm-2. Gels were cultured for 24 h at 37 °C/5% CO2 to allow for cell adhesion and equilibrium cell spreading. EC migration was then monitored for 1 h at 5 min intervals in at least three randomly selected locations of each hydrogel formulation using a Zeiss Axiovert microscope. For determination of single cell migration parameters, only cells that remained in isolation (> 100 μm from other cells) were measured. Cell centroid position was determined based on cell outlines using Photoshop. These centroids were then used to calculate the mean-square displacement (MSD) for a range of time intervals. The speed, S, and direction persistence time (P) were determined by fitting the MSD ($\langle d^2 \rangle$) and the time interval, t, to the persistent random walk equation: using nonlinear least squares regression analysis:

$$\langle d^2 \rangle = 2S^2P[t - P\left(1 - e^{-\left(\frac{t}{P}\right)}\right)]$$

4.4. RESULTS

4.4.1. Endothelial cell adhesion and spreading

As shown in **Figure 12**, ECs strongly spread on functionalized collagen coated surfaces. Furthermore, functionalized Scl2-2 and Scl2-3 coated surfaces mediated EC attachment and spreading whereas EC adhesion on Scl2-1 coated wells was minimal. **Figure 13** shows EC adhesion and spreading on functionalized Scl2 versus collagen on both coated tissue culture polystyrene and PEGDA-Scl2 hydrogels. In the case of coated surfaces, EC adhesion to Scl2-2, Scl2-3 and collagen was significantly higher than what was found for the negative control. Additionally, cell spreading was significantly higher in Scl2-2 and collagen samples relative to the BSA negative controls. On the other hand, regarding hydrogel surfaces, EC adhesion and spreading on Scl2-2, Scl2-3 and collagen was significantly higher than their PEGDA negative controls. Collectively, these results indicate that Scl2-2 and Scl2-3 appear to mediate the attachment and spreading of ECs on polystyrene as well as on hydrogel surfaces.

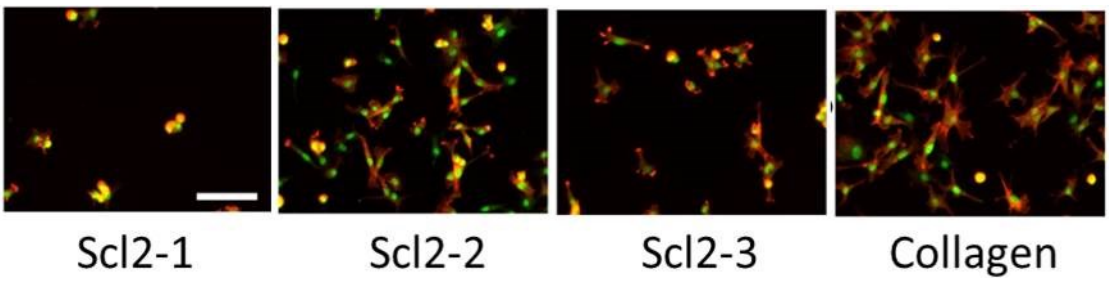

Figure 12. High binding polystyrene 96 well plates were coated with PEG-functionalized Scl2-1, Scl2-2, Scl2-3, and functionalized type I collagen at 1 μg protein per well. ECs were seeded at a density of 20000 cells/cm2 and allowed to spread for 3 hours. Scale bar applies to all images and equals 100 μm.

4.4.2. Endothelial cell migration

The migration of endothelial cells is one of the most relevant processes in vasculogenesis. In the absence of preexisting vessels, they are derived from endothelial precursors . The endothelial cells that contribute to the primary vascular plexus are initially scattered and eventually assemble following migration, at the location of the developing vessel. Therefore, in addition to providing biocompatibility and supporting osteoinductivity, PEGDA-Scl2 hydrogels must be able to promote EC migration. As an initial evaluation of the potential of PEGDA-Scl2-2 gels to promote EC migration, the movements of ECs seeded onto PEGDA-Scl2-2 hydrogels were tracked over 1 hour and PEGDA-Scl2-2 and PEGDA-collagen hydrogels was unaffected by a 2 fold increase in protein concentration, and average EC spreading on PEGDA-Scl2-2 hydrogels was lower than that supported by the PEG-collagen controls, **Figure 15A**. However, EC migration rates on the hydrogels were affected by both type and concentration of protein, **Figure 15B**. Specifically, an increase in the concentration of Scl2-2 from 6 to 12 mg of compared to those on PEGDA-collagen hydrogels, **Figure 14**. EC spreading on both protein per ml of hydrogel solution resulted in a 3 fold increase in EC migration rates from 4.2 ± 2.2 μm min-1 to 13.2 ± 4.2 μm min-1. A corresponding increase in collagen concentration (2 to 4 mg of protein per ml, based on an equivalent number of binding sites relative to 6 and 12 mg of Scl2-2 per mL), did not cause a significant increase in migration rates. Additionally, migration speeds on PEGDA-Scl2-2 hydrogels were increased relative to those on equivalent PEGDA-collagen hydrogels. As cell spreading

increases, the resulting increased contact area generally enhances cell ability to resist detachment.

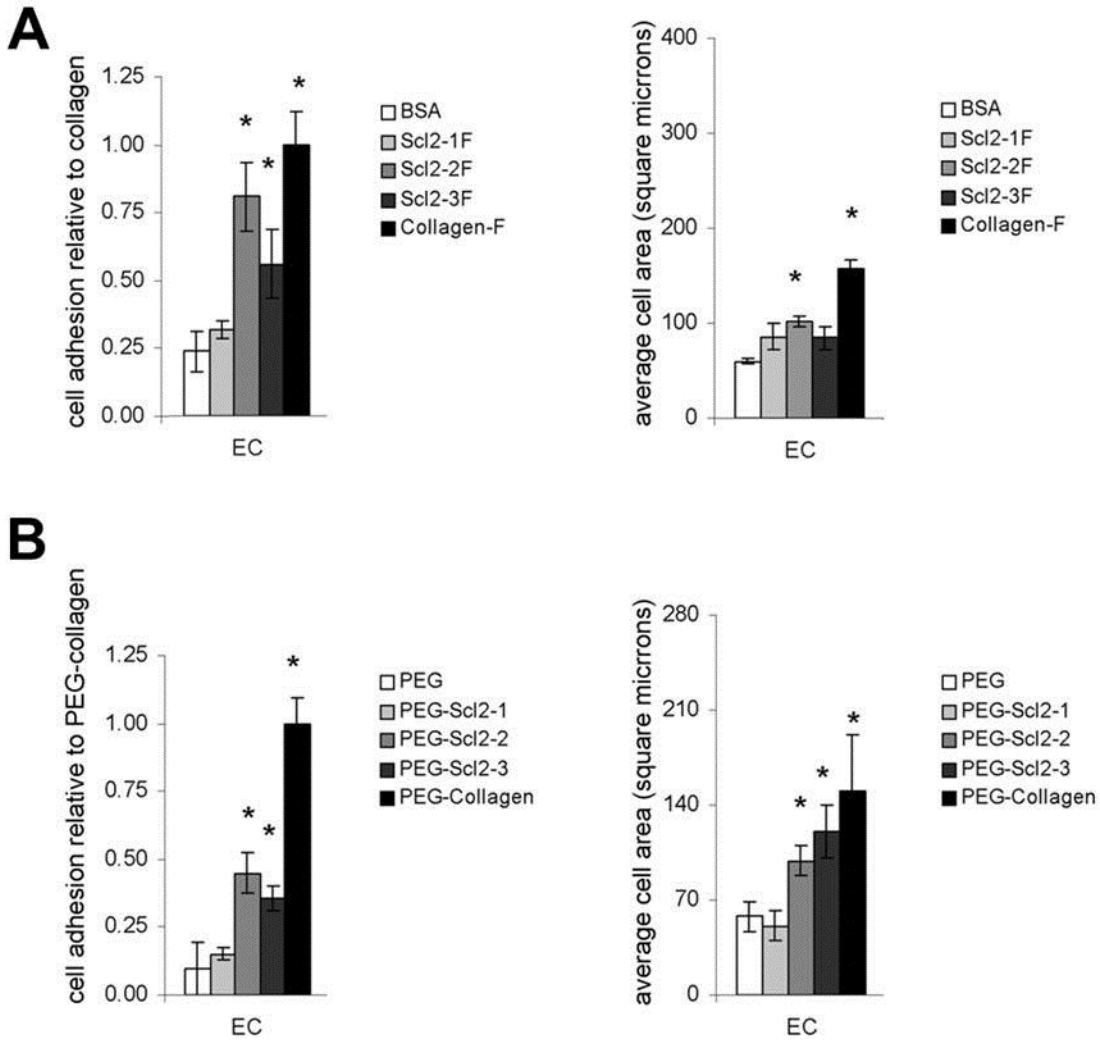

Figure 13. Relative cell adhesion and spreading on functionalized Scl2 versus collagen on coated tissue culture polystyrene (A) and PEGDA-Scl2 hydrogels (B). *, indicates a statistically significant different with the corresponding control (BSA for A and PEG for B), $p < 0.05$.

Therefore, cell spreading can be used as a preliminary indication of adhesion strength on a surface. From this, it can be inferred that ECs on the 12 mg Scl2-2 ml-1 surface had

similar adhesion strength to those on the 6 mg Scl2-2 ml-1 surface while achieving higher migration rates. These studies demonstrated that Scl2-2 concentration can be used to control EC migration rates, and PEGDA-Scl2-2 hydrogels have the potential to improve upon the rate of EC migration relative to collagen-based systems. Future studies will include the use of human ECs rather than bovine ECs.

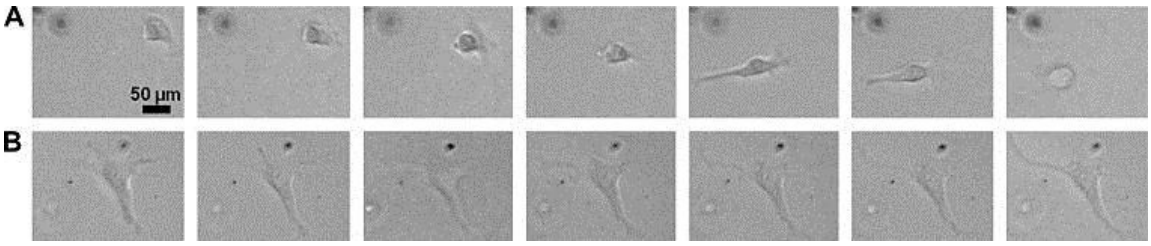

Figure 14. Micrographs used to track endothelial cell centroid position to determine migration rates on (A) PEG-Scl2-2 hydrogels and (B) PEG-collagen hydrogels. The scale bar applies to all images, and images are shown at 10 min intervals.

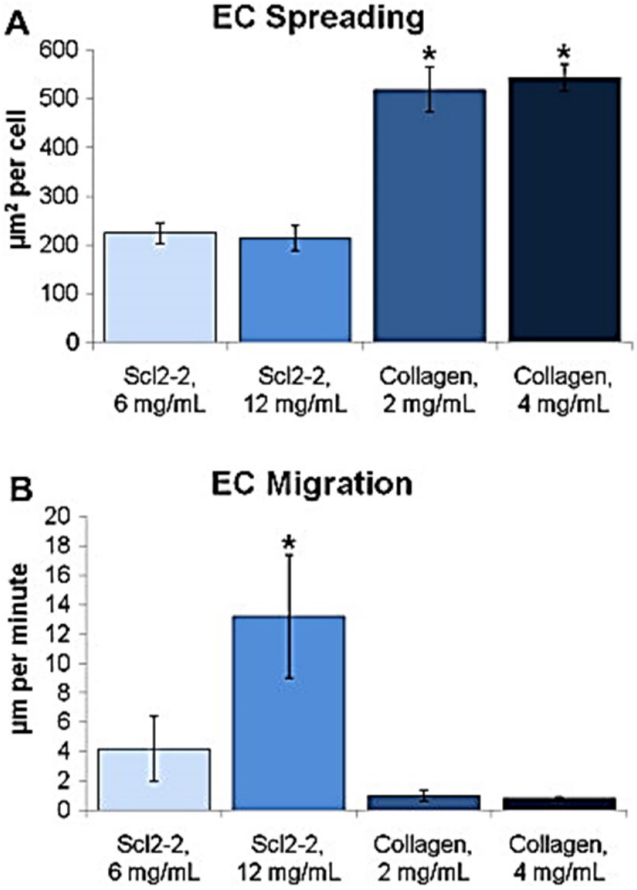

Figure 15. Endothelial cell spreading (A) and rate of EC migration (B). Levels of EC spreading on PEG-collagen hydrogels are approximately twofold higher than on PEG-Scl2-2 hydrogels. EC migration rates increased approximately threefold with increased concentration of Scl2-2, and average migration speeds on Scl2-2 gels were approximately 10-fold greater than those observed on equivalent PEG-collagen gels. n = 6; mean ± standard error of mean displayed; ∗ p > 0.05 relative to 6 mg Scl2-2 ml−1 sample.

4.5. CONCLUSIONS

In the current study, novel PEGDA-Scl2 hydrogel systems were fabricated. In addition to the EC adhesion and spreading experiments on PEGDA-Scl2 hydrogels, the current studies demonstrate that EC migration speed can be tuned on these hydrogels by modulating Scl2-2 concentration. Furthermore, the observed migration speeds were higher than those observed on hydrogels containing equivalent levels of collagen.

Cumulatively, these results indicate that PEGDA-Scl2-2 hydrogels can support EC adhesion, spreading and migration, which are key mechanisms for the generation of blood vessels. In addition to their osteoinductive properties, the fact that our PEGDA-Scl2-2 scaffolds have the ability to support vasculogenesis provides these novel tissue engineering platforms with high potential in the fabrication of improved vascularized bone constructs. Further studies will be conducted using human ECs, instead of BAECs to optimize EC adhesion and migration on PEGDA-Scl2 hydrogels.

CHAPTER V

CONCLUSIONS

The accomplished work represents a contribution towards the development of novel materials that provide enhanced versatility for orthopedic applications. Specifically, evaluation of PAH/PAA coatings on magnetic NiMnSn shape memory alloys indicated that the presence of the polyelectrolyte coatings improved alloy cytocompatibility via reducing ion release. Given that coating stability and integrity are critical to reducing alloy cytotoxicity, the investigation of different methods to improve coating long-term integrity and surface adhesion is indispensable for the design of more biocompatible NiMnSn MSMAs.

On the other hand, in the context of bone regeneration applications, PEGDA based hydrogel systems proved useful tools for the examination of the effect of extracellular matrix (ECM) biomolecules on mesenchymal stem cell (MSC) osteogenic differentiation. Particularly, by using these hydrogel platforms, it was possible to compare the osteoinductivity of ECM proteins that had been previously associated with bone fracture and healing. Present data indicated that both FG and LN enhanced the osteogenic response of encapsulated 10T½ cells. Specifically, osteocalcin levels in day 7 PEG–FG and PEG–LN gels were ~2.4- and 2.9-fold greater, respectively, than day 0 levels. In addition, expression of osterix, an osteoblast-specific transcription factor required for osteogenesis, was significantly elevated in day 7 PEG–LN gels relative to day 0 levels. In contrast, the day 7 levels of markers for adipogenesis, chondrogenesis

and smooth muscle lineage progression were not significantly different among formulations or relative to day 0, indicating that the osteogenic response associated with the PEG–FG and PEG–LN gels was specific. Moreover, further studies conducted in our lab indicated that α1, α2, and α6 integrin mediated adhesion might have strongly influenced the observed differentiation results. Cumulatively, our data indicate that LN may be the most appropriate of the biomolecules examined for promoting specific osteogenic differentiation within the context of scaffolds with osteoinductive moduli. Nonetheless, exploration of a broader range of time points and ECM protein concentrations as well as examination of potential synergy between various ECM components would provide a better understanding of MSC osteogenic responses to specific ECM constituents.

Finally, the ideal system for evaluating the effect of a specific signal on cell behavior should allow the incorporation of the desired signaling in an appropriate three-dimensional (3D) protein structure without the additional signals associated with the biopolymer. Therefore, we employed a novel biomaterial platform based on a collagen-mimetic protein derived from group A Streptococcus, Scl2.28, which maintains the native triple helical structure of native collagen and allows the incorporation of desired integrin-binding motifs. Following the development of two Scl2 proteins, which incorporate α1β1 and/or α2β1 integrin-binding motifs based on the collagen sequences GF/LOGER [7, 8], our lab has been able to show that hybrid PEGDA-Scl2 hydrogels support hMSC osteogenic differentiation. However, since bone replacement materials are more effective if they also support capillary formation in addition to osteogenesis,

we evaluated the ability of PEGDA-Scl2 hybrid scaffolds to support EC adhesion, spreading and migration. Results from these experiments demonstrated that EC migration speed can be tuned on these hydrogels by modulating Scl2-2 concentration. Furthermore, the observed migration speeds were higher than those observed on hydrogels containing equivalent levels of collagen. Cumulatively, these results indicate that PEGDA-Scl2-2 hydrogels can support EC adhesion, spreading and migration, which are key mechanisms for the generation of blood vessels. In addition to their osteoinductive properties, the fact that our PEGDA-Scl2-2 scaffolds have the ability to support vasculogenesis will provide a more controlled platform which will serve as a foundation for the fabrication of more efficient vascularized bone constructs for orthopedic applications.

REFERENCES

[1] Martins-Green M, Hanafusa H. The 9E3/CEF4 gene and its product the chicken chemotactic and angiogenic factor (cCAF): potential roles in wound healing and tumor development. Cytokine Growth Factor Reviews 1997;8:221-32.

[2] Benoit DS, Schwartz M.P, Durney A.R, Anseth K.S. Small functional groups for controlled differentiation of hydrogel-encapsulated human mesenchymal stem cells. Nature Materials 2008;7:816-23.

[3] Ayala R, Zhang C, Yang D, Hwang Y, Aung A, Shroff S.S, et al. Engineering the cell-material interface for controlling stem cell adhesion, migration, and differentiation. Biomaterials 2011;32:3700-11.

[4] Burdick J.A, Anseth K.S. Photoencapsulation of osteoblasts in injectable RGD-modified PEG hydrogels for bone tissue engineering. Biomaterials 2002;23:4315-23.

[5] Yang F, Williams C.G, Wang D.A, Lee H, Manson P.N, Elisseeff J. The effect of incorporating RGD adhesive peptide in polyethylene glycol diacrylate hydrogel on osteogenesis of bone marrow stromal cells. Biomaterials 2005;26:5991-8.

[6] Gombotz W.R, Wang G.H, Horbett T.A, Hoffman A.S. Protein adsorption to poly(ethylene oxide) surfaces. Journal of Biomedical Materials Research 1991;25:1547-62.

[7] Xu Y, Gurusiddappa S, Rich R.L, Owens R.T, Keene D.R, Mayne R, et al. Multiple binding sites in collagen type I for the integrins α1β1 and α2β1. Journal of Biological Chemistry 2000;275:38981-9.

[8] Kim J.K, Xu Y, Xu X, Keene D.R, Gurusiddappa S, Liang X, et al. A novel binding site in collagen type III for integrins α1β1 and α2β1. Journal of Biological Chemistry 2005;280:32512-20.

[9] Koob S, Torio-Padron N, Stark G.B, Hannig C, Stankovic Z, Finkenzeller G. Bone formation and neovascularization mediated by mesenchymal stem cells and endothelial cells in critical-sized calvarial defects. Tissue Engineering Part A 2011;17:311-21.

[10] Tsigkou O, Pomerantseva I, Spencer J.A, Redondo P.A, Hart A.R, O'Doherty E, et al. Engineered vascularized bone grafts. Proceedings of the National Academy of Sciences 2010;107:3311-6.

[11] Karaman I, Karaca H.E, Karsilayan A.I, and Chumlyakov Y.I. Energy harvesting using martensite variant reorientation mechanism in a NiMnGa magnetic shape memory alloy. Applied Physics Letters 2007;90.

[12] El Feninat F, Laroche G, Fiset M, Mantovani D. Shape memory materials for biomedical applications. Advanced Engineering Materials 2002;4:91-104.

[13] Epps J.J, Chopra I. In-flight tracking of helicopter rotor blades using shape memory alloy actuators. Smart Materials and Structures 2001;10:104.

[14] Olson G.B. Martensite and life: displacive transformations as biological processes. Journal de Physique Archives 1982;43:855-65.

[15] Otsuka C.M. Shape memory materials. Cambridge, New York: Cambridge University Press 1998.

[16] Singh K, Sirohi J, Chopra I. An improved shape memory alloy actuator for rotor blade tracking. Journal of Intelligent Material Systems and Structures 2003;14:767-86.

[17] Murray S.J, Kukla A.M, Robinson J, O'Handley R.C, Allen S.M. Large field induced strain in single crystalline Ni–Mn–Ga ferromagnetic shape memory alloy. Applied Physics 2000;87.

[18] Marioni M.A, O'Handley R.C, Allen S.M, Hall S.R, Paul D.I, Richard M.L, et al. The ferromagnetic shape-memory effect in Ni–Mn–Ga. Journal of Magnetism and Magnetic Materials 2005;290–291, Part 1:35-41.

[19] Karaca H.E, Karaman I, Basaran B, Chumlyakov Y.I, Maier H.J. Magnetic field and stress induced martensite reorientation in NiMnGa ferromagnetic shape memory alloy single crystals. Acta Materialia 2006;54:233-45.

[20] Suorsa I, Pagounis E, Ullakko K. Magnetic shape memory actuator performance. Journal of Magnetism and Magnetic Materials 2004;272–276, Part 3:2029-30.

[21] James R.D, Tickle R, Wuttig M. Large field-induced strains in ferromagnetic shape memory materials. Materials Science and Engineering: A 1999;273–275:320-5.

[22] Dapino M.J. On magnetostrictive materials and their use in adaptive structures. Structural Engineering and Mechanics 2004;17:303-29.

[23] Pouponneau P, Savadogo O, Napporn T, Yahia L.H, Martel S. Corrosion study of single crystal Ni–Mn–Ga alloy and Tb0.27Dy0.73Fe1.95 alloy for the design of new medical microdevices. Journal of Materials Science: Materials in Medicine 2011;22:237-45.

[24] Söderberg O, Ge Y, Sozinov A, Hannula S.P, Lindroos V.K. Recent breakthrough development of the magnetic shape memory effect in Ni–Mn–Ga alloys. Smart Materials and Structures 2005;14:S223.

[25] Liu X.W, Ge Y, Lanska N, Ullakko K, Lindroos V.K. On the corrosion of non-stoichiometric martensitic Ni–Mn–Ga alloys. Journal de Physique IV 2003;112:935–38.

[26] Sozinov A, Lanska N, and Ullakko K. Giant magnetic-field-induced strain in NiMnGa seven-layered martensitic phase. Applied Physics Letters 2002;80:1746.

[27] Stepan L.D, Gans E, Mohanchandra K.P, Ujihara M, Carman G.P. Biocorrosion investigation of two shape memory nickel based alloys: Ni–Mn–Ga and thin film NiTi. Journal of Biomedical Materials Research A 2007;82:768–76.

[28] Straka L, Heczko O. Magnetic anisotropy in Ni-Mn-Ga martensites. Journal of Applied Physics 2003;93:8636-8.

[29] Schlagel D.L, Wu Y.L, Zhang W, Lograsso T.A. Chemical segregation during bulk single crystal preparation of Ni–Mn–Ga ferromagnetic shape memory alloys. Journal of Alloys and Compounds 2000;312:77-85.

[30] Wedel C, Itagaki K. High-temperature phase relations in the ternary Ga-Mn-Ni system. Journal of Phase Equilibria 2001;22:324-30.

[31] Karaca H.E, Karaman I, Basaran B, Ren Y, Chumlyakov Y.I, Maier H.J. Magnetic field-induced phase transformation in NiMnCoIn magnetic shape-memory alloys—A new actuation mechanism with large work output. Advanced Functional Materials 2009;19:983-98.

[32] Sutou Y, Koeda Y.I, Omori T, Kainuma R, Ishida K, and Oikawa K. Magnetic and martensitic transformations of NiMnX(X=In,Sn,Sb) ferromagnetic shape memory alloys. Applied Physics Letters 2004;85.

[33] Ito K, Ito W, Umetsu R.Y, Tajima S, Kawaura H, Kainuma R, et al. Metamagnetic shape memory effect in polycrystalline NiCoMnSn alloy fabricated by spark plasma sintering. Scripta Materialia 2009;61:504-7.

[34] Ito K, Ito W, Umetsu R.Y, Karaman I, Ishida K, Kainuma R. Mechanical and shape memory properties of Ni43Co7Mn39Sn11 alloy compacts fabricated by pressureless sintering. Scripta Materialia 2010;63:1236-9.

[35] Pouponneau P, Merhi Y, Mery L, and Martel S. Biocompatibility of candidate materials for the realization of medical microdevices. Proceedings of the 28th IEEE EMBS Annual International Conference, New York City, 2006.

[36] Chatterjee S, De S.K, Majumdar S. Magnetic investigations on Ni-Mn-Sn ferromagnetic shape memory alloy. Advanced Materials Research 2008;52:215-20.

[37] Pulido M.D, Parrish A.R. Metal-induced apoptosis: mechanisms. Mutation Research/Fundamental and Molecular Mechanisms of Mutagenesis 2003;533:227-41.

[38] Hartwig A, Krüger I, Beyersmann D. Mechanisms in nickel genotoxicity: the significance of interactions with DNA repair. Toxicology Letters 1994;72:353-8.

[39] Sullivan M, Pirotta S, Shah A, Wu G, Chopra H.D. In situ study of temperature dependent magnetothermoelastic correlated behavior in ferromagnetic shape memory alloys. Applied Physics 2004;95:6951.

[40] Putters J.L, Kaulesar D.M, de Zeeuw G.R, Bijma A, Besselink P.A. Comparative cell culture effects of shape memory metal (Nitinol), nickel and titanium: a biocompatibility estimation. European Surgical Research 1992;24:378-82.

[41] Laing P.G, Ferguson A.B, Hodge E.S. Tissue reaction in rabbit muscle exposed to metallic implants. Journal of Biomedical Materials Research 1967;1:135-49.

[42] Crossgrove J, Zheng W. Manganese toxicity upon overexposure. NMR in Biomedicine 2004;17:544-53.

[43] Keen C.L, Clegg MS. Manganese and its role in biological processes. New York, Marcel Deker 2000;89.

[44] Yamamoto A, Honma R, Sumita M. Cytotoxicity evaluation of 43 metal salts using murine fibroblasts and osteoblastic cells. Journal of Biomedical Materials Research 1998;39:331-40.

[45] Brown P.J, Gandy A.P, Ishida K, Kainuma R, Kanomata T, Neumann K.U, et al. The magnetic and structural properties of the magnetic shape memory compound Ni 2 Mn 1.44 Sn 0.56. Journal of Physics: Condensed Matter 2006;18:2249.

[46] Santos J.D, Alvarez P, Sanchez M.L, Sánchez J.L, Hernando B, Escoda L.l, Suñol J. J, and Varga R. Microstructure and magnetic properties of Ni50Mn37Sn13 Heusler alloy ribbons. Applied Physics 2008;103.

[47] El Medawar L, Rocher P, Hornez J.C, Traisnel M, Breme J, Hildebrand H.F. Electrochemical and cytocompatibility assessment of NiTiNOL memory shape alloy for orthodontic use. Biomolecular Engineering 2002;19:153-60.

[48] Bryant S.J, Nuttelman C.R, Anseth K.S. Cytocompatibility of UV and visible light photoinitiating systems on cultured NIH/3T3 fibroblasts in vitro. Journal Of Biomaterials Science-Polymer Edition 2000;11:439-57.

[49] Cui Z.D, Chen M.F, Zhang L.Y, Hu R.X, Zhu S.L, Yang X.J. Improving the biocompatibility of NiTi alloy by chemical treatments: An in vitro evaluation in 3T3 human fibroblast cell. Materials Science and Engineering: C 2008;28:1117-22.

[50] Bogdanski D, Koller M, Muller D, Muhr G, Bram M, Buchkremer H.P, et al. Easy assessment of the biocompatibility of Ni-Ti alloys by in vitro cell culture experiments on a functionally graded Ni-NiTi-Ti material. Biomaterials 2002;23:4549-55.

[51] Dai J, Sullivan D.M, Bruening M.L. Ultrathin, layered polyamide and polyimide coatings on aluminum. Industrial & Engineering Chemistry Research 2000;39:3528-35.

[52] Hoffmann K, Friedrich T, Tieke B. Layer-by-layer assembled polyelectrolyte blend membranes and their use for ion separation and rejection. Polymer Engineering & Science 2011;51:1497-506.

[53] Lackmann J, Regenspurger R, Maxisch M, Grundmeier G, Maier H.J. Defect formation in thin polyelectrolyte films on polycrystalline NiTi substrates. Journal of the Mechanical Behavior of Biomedical Materials 2010;3:436-45.

[54] Lackmann J, Maxisch M, Regenspurger R, Grundmeier G. Formability of thermally cured and of nanoclay-reinforced polyelectrolyte films on NiTi substrates. Materials Science 2012;47:151-61.

[55] Bryant S.J, Nuttelman C.R, Anseth K.S. Cytocompatibility of UV and visible light photoinitiating systems on cultured NIH/3T3 fibroblasts in vitro. Journal of Biomaterials Science 2000;11:439-57.

[56] Bryant S.J, Anseth K.S. Hydrogel properties influence ECM production by chondrocytes photoencapsulated in poly(ethylene glycol) hydrogels. Journal of Biomedical Materials Research 2002;59:63-72.

[57] Williams C.G, Malik A.N, Kim T.K, Manson P.N, Elisseeff J.H. Variable cytocompatibility of six cell lines with photoinitiators used for polymerizing hydrogels and cell encapsulation. Biomaterials 2005;26:1211-8.

[58] Munoz-Pinto D.J, Jimenez-Vergara A.C, Gelves L.M, McMahon R.E, Guiza-Arguello V, Hahn M.S. Probing vocal fold fibroblast response to hyaluronan in 3D contexts. Biotechnology and Bioengineering 2009;104:821-31.

[59] Doyle A.D, Wang F.W, Matsumoto K, Yamada K.M. One-dimensional topography underlies three-dimensional fibrillar cell migration. The Journal of Cell Biology 2009;184:481-90.

[60] Li L, Lu Y. Optimizing a 3D culture system to study the interaction between epithelial breast cancer and its surrounding fibroblasts. Journal of Cancer 2011;2:458-66.

[61] Harris J.J, DeRose P.M, Bruening M.L. Synthesis of passivating, nylon-like coatings through cross-linking of ultrathin polyelectrolyte films. Journal of the American Chemical Society 1999;121:1978-9.

[62] Kundu A.K, Putnam A.J. Vitronectin and collagen I differentially regulate osteogenesis in mesenchymal stem cells. Biochemical Biophysical Research Communications 2006;347:347-57.

[63] Kundu A.K, Khatiwala C.B, Putnam A.J. Extracellular matrix remodeling, integrin expression, and downstream signaling pathways influence the osteogenic differentiation of mesenchymal stem cells on poly(lactide-co-glycolide) substrates. Tissue Engineering Part A 2009;15:273-83.

[64] Salasznyk R.M, Williams W.A, Boskey A, Batorsky A, Plopper G.E. Adhesion to vitronectin and collagen I promotes osteogenic differentiation of human mesenchymal stem cells. Journal of Biomedicine and Biotechnology 2004;2004:24-34.

[65] Klees R.F, Salasznyk R.M, Kingsley K, Williams W.A, Boskey A, Plopper G.E. Laminin-5 induces osteogenic gene expression in human mesenchymal stem cells through an ERK-dependent pathway. Molecular Biology of the Cell 2005;16:881-90.

[66] Salasznyk R.M, Klees R.F, Hughlock M.K, Plopper G.E. ERK signaling pathways regulate the osteogenic differentiation of human mesenchymal stem cells on collagen I and vitronectin. Cell Communication Adhesion 2004;11:137-53.

[67] Xiao G, Gopalakrishnan R, Jiang D, Reith E, Benson M.D, Franceschi R.T. Bone morphogenetic proteins, extracellular matrix, and mitogen-activated protein kinase signaling pathways are required for osteoblast-specific gene expression and differentiation in MC3T3-E1 cells. Journal of Bone Mineral Research 2002;17:101-10.

[68] Xiao G, Wang D, Benson M.D, Karsenty G, Franceschi R.T. Role of the alpha2-integrin in osteoblast-specific gene expression and activation of the Osf2 transcription factor. Journal of Biological Chemistry 1998;273:32988-94.

[69] Salasznyk R.M, Klees R.F, Boskey A, Plopper G.E. Activation of FAK is necessary for the osteogenic differentiation of human mesenchymal stem cells on laminin-5. Journal of Cell Biochemistry 2007;100:499-514.

[70] Klees R.F, Salasznyk R.M, Ward D.F, Crone D.E, Williams W.A, Harris M.P, et al. Dissection of the osteogenic effects of laminin-332 utilizing specific LG domains: LG3 induces osteogenic differentiation, but not mineralization. Experimental Cell Research 2008;314:763-73.

[71] Huang C.H, Chen M.H, Young T.H, Jeng J.H, Chen Y.J. Interactive effects of mechanical stretching and extracellular matrix proteins on initiating osteogenic

differentiation of human mesenchymal stem cells. Journal of Cell Biochemistry 2009;108:1263-73.

[72] Salasznyk R.M, Klees R.F, Williams W.A, Boskey A, Plopper G.E. Focal adhesion kinase signaling pathways regulate the osteogenic differentiation of human mesenchymal stem cells. Experimental Cell Research 2007;313:22-37.

[73] Takeuchi Y, Nakayama K, Matsumoto T. Differentiation and cell surface expression of transforming growth factor-beta receptors are regulated by interaction with matrix collagen in murine osteoblastic cells. Journal of Biological Chemistry 1996;271:3938-44.

[74] Lund A.W, Stegemann J.P, Plopper G.E. Inhibition of ERK promotes collagen gel compaction and fibrillogenesis to amplify the osteogenesis of human mesenchymal stem cells in three-dimensional collagen I culture. Stem Cells and Development 2009;18:331-41.

[75] Benoit D.S, Durney A.R, Anseth K.S. The effect of heparin-functionalized PEG hydrogels on three-dimensional human mesenchymal stem cell osteogenic differentiation. Biomaterials 2007;28:66-77.

[76] Hwang N.S, Varghese S, Li H, Elisseeff J. Regulation of osteogenic and chondrogenic differentiation of mesenchymal stem cells in PEG-ECM hydrogels. Cell Tissue Research 2011;344:499-509.

[77] Parekh S.H, Chatterjee K, Lin-Gibson S, Moore N.M, Cicerone M.T, Young M.F, et al. Modulus-driven differentiation of marrow stromal cells in 3D scaffolds that is independent of myosin-based cytoskeletal tension. Biomaterials 2011;32:2256-64.

[78] Cukierman E, Pankov R, Stevens D.R, Yamada K.M. Taking cell-matrix adhesions to the third dimension. Science 2001;294:1708-12.

[79] Bissell M.J, Rizki A, Mian I.S. Tissue architecture: the ultimate regulator of breast epithelial function. Current Opinion in Cell Biology 2003;15:753-62.

[80] Huebsch N, Arany P.R, Mao A.S, Shvartsman D, Ali O.A, Bencherif S.A, et al. Harnessing traction-mediated manipulation of the cell/matrix interface to control stem-cell fate. Nature Materials 2010;9:518-26.

[81] Weiss R.E, Reddi A.H. Appearance of fibronectin during the differentiation of cartilage, bone, and bone marrow. Journal of Cell Biology 1981;88:630-6.

[82] Foidart J.M, Reddi A.H. Immunofluorescent localization of type IV collagen and laminin during endochondral bone differentiation and regulation by pituitary growth hormone. Developmental Biology 1980;75:130-6.

[83] Klotch D.W, Ganey T.M, Slater-Haase A, Sasse J. Assessment of bone formation during osteoneogenesis: a canine model. Otolaryngology Head Neck Surgery 1995;112:291-302.

[84] Bulick A.S, Munoz-Pinto D.J, Qu X, Mani M, Cristancho D, Urban M, et al. Impact of endothelial cells and mechanical conditioning on smooth muscle cell extracellular matrix production and differentiation. Tissue Engineering Part A 2009;15:815-25.

[85] Hummon A.B, Lim S.R, Difilippantonio M.J, Ried T. Isolation and solubilization of proteins after TRIzol extraction of RNA and DNA from patient material following prolonged storage. Biotechniques 2007;42:467-70, 72.

[86] Watkins A.W, Anseth K.S. Investigation of molecular transport and distributions in poly(ethylene glycol) hydrogels with confocal laser scanning microscopy. Macromolecules 2005;38:1326-34.

[87] Armstrong J.K, Wenby R.B, Meiselman H.J, Fisher T.C. The hydrodynamic radii of macromolecules and their effect on red blood cell aggregation. Biophysical Journal 2004;87:4259-70.

[88] Buxton A.N, Zhu J, Marchant R, West J.L, Yoo J.U, Johnstone B. Design and characterization of poly(ethylene glycol) photopolymerizable semi-interpenetrating networks for chondrogenesis of human mesenchymal stem cells. Tissue Engineering 2007;13:2549-60.

[89] Munoz-Pinto D.J, Jimenez-Vergara A.C, Gelves L.M, McMahon R.E, Guiza-Arguello V, Hahn M.S. Probing vocal fold fibroblast response to hyaluronan in 3D contexts. Biotechnology and Bioengineering 2009;104:821-31.

[90] Munoz-Pinto D.J, Bulick A.S, Hahn M.S. Uncoupled investigation of scaffold modulus and mesh size on smooth muscle cell behavior. Journal of Biomedical Materials Research A 2009;90:303-16.

[91] Gregory T.R. Nucleotypic effects without nuclei: genome size and erythrocyte size in mammals. Genome 2000;43:895-901.

[92] Salinas C.N, Anseth K.S. The influence of the RGD peptide motif and its contextual presentation in PEG gels on human mesenchymal stem cell viability. Journal of Tissue Engineering and Regenerative Medicine 2008;2:296-304.

[93] Salinas C.N, Anseth K.S. The enhancement of chondrogenic differentiation of human mesenchymal stem cells by enzymatically regulated RGD functionalities. Biomaterials 2008;29:2370-7.

[94] Liao H, Munoz-Pinto D, Qu X, Hou Y, Grunlan M.A, Hahn M.S. Influence of hydrogel mechanical properties and mesh size on vocal fold fibroblast extracellular matrix production and phenotype. Acta Biomaterialia 2008;4:1161-71.

[95] Bryant S.J, Anseth K.S. Controlling the spatial distribution of ECM components in degradable PEG hydrogels for tissue engineering cartilage. Journal of Biomedical Materials Research A 2003;64:70-9.

[96] Bryant S.J, Durand K.L, Anseth K.S. Manipulations in hydrogel chemistry control photoencapsulated chondrocyte behavior and their extracellular matrix production. Journal of Biomedical Materials Research A 2003;67:1430-6.

[97] Peyton S.R, Raub C.B, Keschrumrus V.P, Putnam A.J. The use of poly(ethylene glycol) hydrogels to investigate the impact of ECM chemistry and mechanics on smooth muscle cells. Biomaterials 2006;27:4881-93.

[98] Jimenez-Vergara A.C, Munoz-Pinto D.J, Becerra-Bayona S, Wang B, Iacob A, Hahn M.S. Influence of glycosaminoglycan identity on vocal fold fibroblast behavior. Acta Biomaterialia 2011;7:3964-72.

[99] Steinmetz N.J, Bryant S.J. The effects of intermittent dynamic loading on chondrogenic and osteogenic differentiation of human marrow stromal cells encapsulated in RGD-modified poly(ethylene glycol) hydrogels. Acta Biomaterialia 2011;7:3829-40.

[100] Nuttelman C.R, Tripodi M.C, Anseth K.S. Synthetic hydrogel niches that promote hMSC viability. Matrix Biology 2005;24:208-18.

[101] Salasznyk R.M, Williams W.A, Boskey A, Batorsky A, Plopper G.E. Adhesion to vitronectin and collagen I promotes osteogenic differentiation of human mesenchymal stem cells. Journal of Biomedical Biotechnology 2004;2004:24-34.

[102] Karp J.M, Sarraf F, Shoichet M.S, Davies J.E. Fibrin-filled scaffolds for bone-tissue engineering: An in vivo study. Journal of Biomedical Materials Research A 2004;71:162-71.

[103] Le Nihouannen D, Guehennec L.L, Rouillon T, Pilet P, Bilban M, Layrolle P, et al. Micro-architecture of calcium phosphate granules and fibrin glue composites for bone tissue engineering. Biomaterials 2006;27:2716-22.

[104] Peled E, Boss J, Bejar J, Zinman C, Seliktar D. A novel poly(ethylene glycol)-fibrinogen hydrogel for tibial segmental defect repair in a rat model. Journal of Biomedical Materials Research A 2007;80:874-84.

[105] Mulliken J.B, Kaban L.B, Glowacki J. Induced osteogenesis--the biological principle and clinical applications. Journal of Surgery Research 1984;37:487-96.

[106] Schlag G, Redl H. Fibrin sealant in orthopedic surgery. Clinical Orthopaedics and Related Research 1988;227:269-85.

[107] Le Guehennec L, Layrolle P, Daculsi G. A review of bioceramics and fibrin sealant. European Cell Materials 2004;8:1-10.

[108] Abiraman S, Varma H.K, Umashankar P.R, John A. Fibrin glue as an osteoinductive protein in a mouse model. Biomaterials 2002;23:3023-31.

[109] Kania R.E, Meunier A, Hamadouche M, Sedel L, Petite H. Addition of fibrin sealant to ceramic promotes bone repair: long-term study in rabbit femoral defect model. Journal of Biomedical Materials Research 1998;43:38-45.

[110] Bensaid W, Triffitt J.T, Blanchat C, Oudina K, Sedel L, Petite H. A biodegradable fibrin scaffold for mesenchymal stem cell transplantation. Biomaterials 2003;24:2497-502.

[111] Cunin G, Boissonnet H, Petite H, Blanchat C, Guillemin G. Experimental vertebroplasty using osteoconductive granular material. Spine (Phila Pa 1976);25:1070-6.

[112] Hayward I.P, Bridle K.R, Campbell G.R, Underwood P.A, Campbell J.H. Effect of extracellular matrix proteins on vascular smooth muscle cell phenotype Cell Biology International 1995;19:727-34.

[113] Humtsoe J.O, Kim J.K, Xu Y, Keene D.R, Hook M, Lukomski S, et al. A streptococcal collagen-like protein interacts with the α2β1 integrin and induces intracellular signaling. Journal of Biological Chemistry 2005;280:13848-57.

[114] Caswell C.C, Barczyk M, Keene D.R, Lukomska E, Gullberg D.E, Lukomski S. Identification of the first prokaryotic collagen sequence motif that mediates binding to human collagen receptors, integrins α2β1 and α1β1. Journal of Biological Chemistry 2008;283:36168-75.

[115] Hahn M.S, Miller J.S, West J.L. Three-dimensional biochemical and biomechanical patterning of hydrogels for guiding cell behavior. Advanced Materials 2006;18:2679-84.

[116] Mann B.K, West J.L. Cell adhesion peptides alter smooth muscle cell adhesion, proliferation, migration, and matrix protein synthesis on modified surfaces and in polymer scaffolds. Journal of Biomedical Materials Research 2002;60:86-93.

[117] Cosgriff-Hernandez E, Hahn M, Wilems T, Munoz-Pinto D.J, Browning M, Rivera J, et al. Bioactive hydrogels based on designer collagens. Acta Biomaterialia 2010;18:2315-21.

[118] Sebra R, Masters K, Bowman C, Anseth K. Surface grafted antibodies: controlled architecture permits enhanced antigen detection. Langmuir 2005;21:10907-11.

[119] Hahn M.S, Taite L.J, Moon J.J, Rowland M.C, Ruffino K.A, West J.L. Photolithographic patterning of polyethylene glycol hydrogels. Biomaterials 2006;27:2519-24.

[120] Douglas J, Poole T.J. Endothelial cell origin and migration in embryonic heart and cranial blood vessel development. The Anatomical Record 1991;231:383-95.